UNIVERSITÀ DEGLI STUDI DI PADOVA

Dipartimento di Fisica e Astronomia "Galileo Galilei"

Corso di Laurea Magistrale in Fisica

Tesi di Laurea

Fluidization of concentrated emulsions in herringbones decorated microfluidic channels

Relatore

Ch.mo Prof. Matteo Pierno

Controrelatore

Ch.ma Prof.ssa Cinzia Sada

Laureando

Francesco Nalin

Anno Accademico 2017/2018

Contents

List of Figures

Introduction

Physics has always studied the response of materials to external forces. For example, for most solids the applied stress produces elastic deformations, meaning that the materials return to the initial state if the stress is removed. On the contrary, liquids can not sustain a shear stress. However, certain classes of materials show both these behaviours. A toothpaste flows like a liquid through the squeezed tube and spreads over the toothbrush where it will remain at rest while the brush is brought up to the mouth. Mayonnaise, that is prepared by strong mixing of two immiscible fluids, it can be dispersed over a food surface and it will remain at rest there. Tooth-paste and mayonnaise are just two examples of substances thus present intermediate behaviour between solid and liquid state; others examples include: emulsions, gels, creams, pastes, foams and muds.

To understand whether a (soft) material can flow as a viscous liquid or stay ad rest as an amorphous solid, it is necessary to have a look at the dynamics of its constituents (i.e. droplets for emulsions, bubbles for foams, blobs for gels, etc.). At the micro-scale these materials are in jammed state [1, 2]: meaning that the constitutive particles are caged by their neighbors. So that, at rest, their dynamics is so limited that the whole system can be considered "dynamic arrested" which is characteristic of many glasses materials, either soft or hard.

At the microscale, the response of these materials to an external stress can be described by successive steps of elastic deformation and plastic rearrangements. During the elastic deformation, the particles remain trapped in a deformed cage. If the deformation is large enough, the particles will escape from the cage, and the stress due to the deformation will be relaxed. This relaxation is also called local rearrangement. When rearrangement occurs, other rearrangements will occur in the neighbourhood; such cooperation between rearrangements produces a non-local behaviour.

Materials that respond with this non-linear rheological behaviour are called Yield stress fluids. They respond elastically to an external stress, unless a threshold value, called Yield stress, is reached. Above yield, the material starts to flow. The characteristic rheological relationship stress vs. shear rate, is given by the Hershel-Bulkley model [3–5]. This solid-to-liquid transition and the corresponding flowing properties have been widely studied [6–9]. However, controlling their dynamics at different scales remains a great challenge for many industrial and technological applications.

By studying the flow of a concentrated emulsion in a rectangular microchannel, Goyon et al. [10] show that the viscosity is not controlled by the bulk rheology but depends on the neighbourhood.

In addition, Mansard [11], Derzsi and Filippi [12, 13] showed that the fluidization of concentrated emulsion can be tuned by suitable wall roughness textured on the channel walls. However, in all these investigations the texturing was symmetric along the cross section of the channels.

In this thesis we address the role of herringbone roughness, introducing a symmetry "rupture" along the cross section.

Thesis outline In the first Chapter we deal with the description of Soft Glassy Materials. To describe them properly, we start with defining Newtonian and non-Newtonian fluids. We describe the categories of fluids which compose the non-Newtonian class, giving examples of the most common behaviours. Then we focus on Yield Stress fluids, with a particular interest for concentrated emulsions, the model of SGM studied in this work.

At this point we start the description of the behaviour of fluids at the microscale, which is very different from the macroscopic behaviour and shows unique effects. We introduce the Navier-Stokes equations that describe the flow, and then we consider these equations for the particular case of parallel plates flow. After that we describe the flow of yield stress fluids in this geometry, and we discuss the role of slip velocity for Soft Glassy Materials. Finally we deal with emulsion rheology, giving an overview on latest results, especially on those that influenced this thesis.

In the second chapter we describe the experimental details of this work. We start this chapter describing the emulsion used for our experiments, giving details on its composition and on the procedures to produce this emulsion. We also describe the process to characterize the emulsion.

Then, we focus on the microfluidic channels created on purpose for this work. We describe their layout and the procedures to prepare them for measures.

At the end of this chapter we introduce the Micro Particle Tracking Velocimetry, i.e. the technique used in this thesis to characterize the flow in channels. The experimental setup is presented, with all the necessary to make the emulsion flow and to record its motion. Then we define the procedure followed to analyse the obtained data.

In the third chapter the experimental results are presented. In particular we could observe that the herringbone roughness has effects on emulsions that are not observed for Newtonian fluids. We describe the effects given by the centrifugation process on the emulsion stored in syringes, since they influenced our procedures. Then we study in deep the effect given by the asymmetric structure, changing also the angle and the gap of the V-shaped grooves, and the pressure drop that enhances the emulsion flow.

At the end of this chapter we discuss the observed effects and we explain them with some physical descriptions.

The last chapter of the thesis is dedicated to the conclusions.

Chapter 1

Soft Glassy Materials

Soft glassy materials (SGMs) are concentrated hard and soft particle assemblies [14]. Some examples of SGMs are gels, foams, pastes, concentrated suspensions and emulsions. SGMs belong to the more general class of materials named *Complex* fluids, including all the mixtures that have a coexistence between two phases.

With a microscopical study, we could observe short range forces, steric forces and polydispersity. All these microscopic features make these fluids difficult to understand. Qualitatively we could say that their flow is different from the flow of simple liquids. For example we could compare an emulsion like mayonnaise with a simple liquid like water and it is easy to see that they flow in a different way, but a quantitative definition is necessary. To describe SGMs quantitatively, we need to introduce rheology, the science that studies how matter flows or deforms in response to applied external forces.

Rheology divides soft materials in two large categories: Newtonian and non-Newtonian fluids. This chapter describes the main properties of these two classes of fluids. In section 1.1 we give a definition of Newtonian fluids and we describe their general behaviour. Non-Newtonian fluids are then described in section 1.2, and we see that there are more categories of non-Newtonian fluids. These categories are described in subsections 1.2.1, 1.2.2 and 1.2.3.

Yield stress fluids are a particular class of fluids that do not flow unless we apply a strong enough stress. In section 1.3 we describe these fluids, and we focus on concentrated emulsions in subsection 1.3.1.

Since we study the emulsion behaviour in microfluidic channels, we need to give a description of fluids at the small scale. In section 1.4 we deal with this topic, introducing microfluidics in subsection 1.4.1, and describing particular cases of interest for this thesis, as the parallel plate flow (1.4.2), the flow of yield stress fluids (1.4.3) and the existence of a wall slip velocity (1.4.4).

In section 1.5 we focus on the rheology of emulsions, and finally we describe concentrated emulsions flow in subsection 1.5.1. In this last section we describe some experimental results that influenced the purpose of this thesis.

§ 1.1. Newtonian Fluids

The Newtonian fluids are described in this section, in order to identify the differences with non-Newtonian ones.
Firstly, it is important to define a flow configuration to study the fluid. Let us consider the sample loaded between two parallel plates with fixed surface S and fixed inter-plane distance h as seen in figure 1.1a.

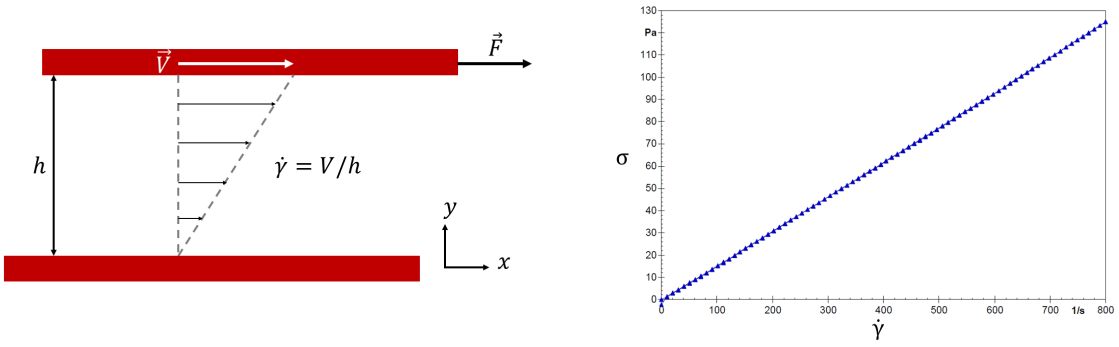

(a) Simple flow configuration

(b) σ vs $\dot{\gamma}$

Figure 1.1 : In figure (a) we can see a scheme for the behaviour of a fluid in a simple flow configuration . In figure (b) is presented a the graph comparing σ and $\dot{\gamma}$ for a Newtonian fluid (glycerol). Picture (b) adapted from [15]

Let us consider a force **F** acting on the top plate, so that the lower plate is motionless and the upper plate is moved with a constant velocity V in the x direction. We could decompose **F** in two component, calling F_t the tangential component and F_n the normal one. The y axis is normal to the plates. Assuming h and S much greater than the characteristic size of the particles of the fluid, it is possible to define quantities uniformly all over the sample. We introduce the shear stress $\sigma = F_t/S$, the normal stress $P = F_n/S$ and the shear rate $\dot{\gamma} = V/h = dV(y)/dy$. At this point we have all the quantities necessary to define a Newtonian fluid in a simple shear system.
A Newtonian fluid is a fluid that shows a linear relation between the stress σ and the shear rate $\dot{\gamma}$ as in the following equation.

$$\sigma = \eta\dot{\gamma} \tag{1.1}$$

The value of proportionality η is called viscosity and it is a constant value for Newtonian fluid at a fixed temperature and pressure.
The viscosity depends on the characteristics of the fluids, such as the molecules weight and the forces acting between molecules. For example the viscosity of air is $\eta \sim 10^{-5}$ Pa s, the viscosity of water is $\eta \sim 10^{-3}$ Pa s and the viscosity of Glycerol is $\eta \sim 1.5$ Pa s. In figure 1.1b we can see an example of rheological curve for Newtonian fluids. The curve represents different values for σ in function of $\dot{\gamma}$ for glycerol. We can see that σ scales linearly with $\dot{\gamma}$, the slope of the line is exactly η. We also define the friction coefficient $\mu = \sigma/P$.

§ 1.2. Non-Newtonian Fluids

The category of non-Newtonian fluids includes all the materials that are not described by equation 1.1. In this way we are including all the materials that do not show a linear relationship between σ and $\dot{\gamma}$, and the materials characterized by a curve for σ vs. $\dot{\gamma}$ not passing through the origin.
If we define the apparent viscosity as $\sigma/\dot{\gamma}$, we can see that for non-Newtonian fluids, this value is not constant. It can depend on the applied stress or on the shear rate, but sometimes it depends also on the history of the fluid. To describe easily non-Newtonian fluids, it is useful to separate them into three categories:

- Time-independent fluids;
- Time-dependent fluids;
- Viscoelastic fluids.

Sometimes it is not easy to divide non-Newtonian fluids in these categories, because their behaviour is common to more categories. In this cases the description is based on the more pronounced non-Newtonian behaviour. In the following paragraphs we focus on the description of these categories.

§ 1.2.1. Time-independent fluids

These fluids are also called generalized Newtonian fluids. For these fluids the value of $\dot{\gamma}$ is always determined by the value of σ and vice versa. In other words, we can describe the strain rate as a function of the stress.

$$\dot{\gamma} = f(\sigma) \quad \text{or} \quad \sigma = f^{-1}(\dot{\gamma}) \tag{1.2}$$

From equation 1.2 we can see that time-independent fluids have no memory of their past history, in fact the dependence is only between $\dot{\gamma}$ and σ. Fluids described by this equation could be divided in three classes.

- Shear- thinning or pseudoplastic;
- Shear- thickening or dilatant;
- Visco-plastic with or without shear-thinning behavior.

These fluids are described in next paragraphs, and we present in figure 1.2 a scheme to describe their behaviour.

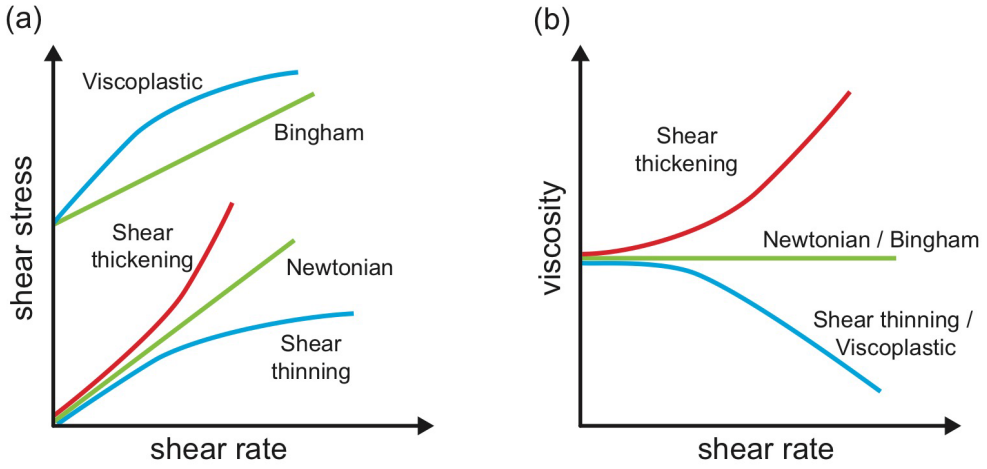

Figure 1.2 : Schemes for for Newtonian and generalized Newtonian fluids. In figure (a) we represent a shear stress vs shear rate curve and in figure (b) the viscosity trend is presented as a function of shear rate.

Shear-thinning fluids These fluids are the more common type of time-independent fluids that could be observed. In this case the apparent viscosity η gradually decreases as the shear rate increases. This means that the fluid flows easily when the shear rate increases. The apparent viscosity changes in relation to the shear rate: at low shear rates its value is practically independent from the shear rate, and the behaviour is similar to the Newtonian fluids, while at higher shear rates the viscosity decreases. In polymer solutions a limit value for the viscosity is observed at very high shear rates i.e. a Newtonian-like plateau where the viscosity does not depend on the shear rate. The lower limit is called η_0 while the upper limit, when it exists, is called η_∞. An example of this behaviour is presented in figure 1.3a. The graph shows the behaviour of a polymer solution. It depicts the viscosity values going from η_0 to η_∞.

Polymer melts, foams or emulsion do not show the viscosity limit value η_∞. Hence, the apparent viscosity for these materials decreases if the shear rate increases, as shown in Fig. 1.3(b) for three pseudoplastic polymer solutions. For these materials the values of η_0 are different for each case, and the viscosity changes in a different way for every system. Obviously the shear stress assumes different values for the three materials. The viscosity behaviour is influenced by different characteristics of the material, so, for polymer solutions, it depends on the selected solvent and on the type of the polymer. Emulsion and suspensions are influenced especially from other factors like the concentration and the particle size or shape [17]. If we want to explain these effects microscopically, we could use schemes represented in figure 1.4. At low shear rates the polymer molecules appear entangled and twisted. As we increase the shear rate, molecules start to disentangle and to stretch on a main direction. When all the molecules are disentangled, the apparent viscosity is increased and the fluid flows easily. To describe shear thinning fluids many models have been presented in years. here we discuss the most common models.

A power law model as the **Ostwald-de Waele** equation (eq. 1.3, [19]) could describe both the shear thinning and the shear thickening fluids, so it is very useful. To describe the fluid we start considering the following expression of σ.

$$\sigma = m(\dot{\gamma})^n \tag{1.3}$$

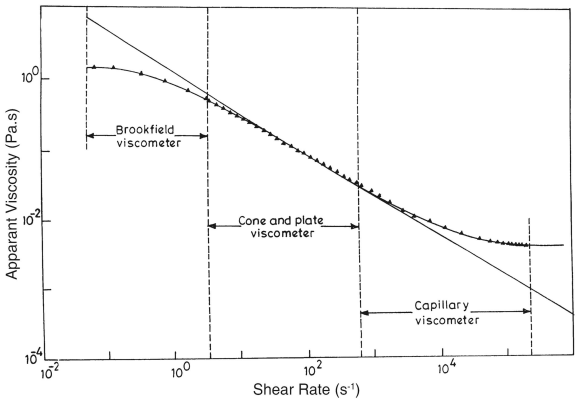

(a) Apparent viscosity for a polymer solution

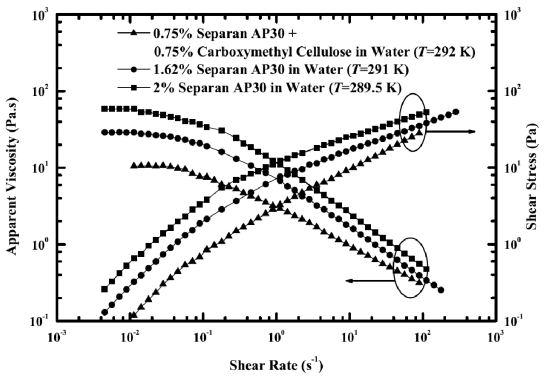

(b) Apparent viscosity and shear stress for pseudoplastic polymer solutions

Figure 1.3 : Figure(a) shows the apparent viscosity η in function of the shear rate $\dot{\gamma}$ for a polymer solution. η_0 and η_∞ are observed. Figure (b) shows the apparent viscosity and the shear stress curves in function of the shear rate for three different pseudoplastic polymer solutions. Pictures are taken from [16].

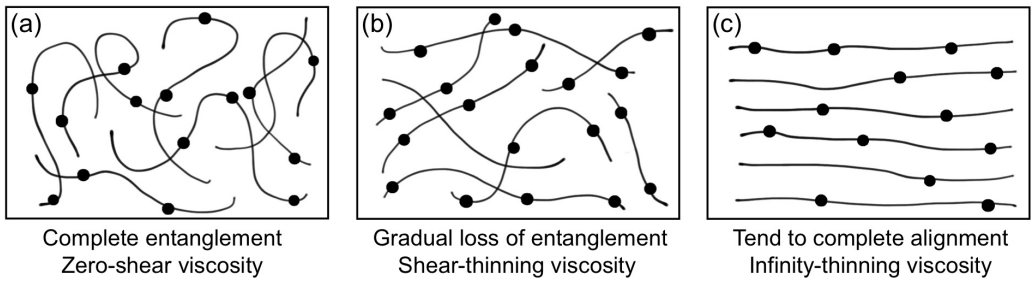

Figure 1.4 : Scheme representing the microscopic behaviour of shear thinning fluids under the increasing of shear. The picture is taken from [18].

so, if we consider the apparent viscosity, we get

$$\eta = m(\dot{\gamma})^{n-1} \tag{1.4}$$

In these equations n is called *flow behaviour index*, while m is called *flow consistency index*.
We can describe a shear thinning fluid if $n < 1$ while shear thickening fluids are described from $n > 1$. If we put $n = 1$ we get the Newtonian fluids. We can see that for small values of n the material has a marked shear thinning behaviour.
Experimental values of n for shear thinning materials are usually included in the range $0.3-0.7$, and they depends on the fluid characteristics as the molecular weight and the concentration of polymers.
The power law approach is slightly different from the effective behaviour of non-Newtonian fluids, in fact it is impossible to predict the Newtonian plateaus (η_0 and η_∞) for small and great values of $\dot{\gamma}$.
It could be corrected with this wide accepted empirical model called **Cross model** [20].

$$\frac{\eta - \eta_\infty}{\eta_0 - \eta_\infty} = \frac{1}{1 + m(\dot{\gamma})^n} \tag{1.5}$$

If $n < 1$ with this model we can predict the shear thinning behaviour. This model is used to fit experimental data and n is usually set as a free parameter to increase the degrees of fit.
An alternative model to describe fluids could be based on the $\dot{\gamma} = f(\sigma)$ representation. For example we describe the **Ellis model** for a unidirectional simple shear

$$\eta = \frac{\eta_0}{1 + (\frac{\sigma}{\sigma_{1/2}})^{\alpha-1}} \tag{1.6}$$

In this equation $\sigma_{1/2}$ and α are two parameters to set in order to obtain the best fit for experimental values.
If we put $\alpha > 1$ then the viscosity decreases as the shear rate increases. The Newtonian limit could be obtained by setting $\sigma_{1/2} \to \infty$, while we could obtain the power law equations (1.3 and 1.4) by setting $(\sigma/\sigma_{1/2}) \gg 1$.

Shear-thickening fluids These fluids are characterized by an increasing of the viscosity as the shear rate increases. Like the pseudoplastic systems, they do not show any yield stress. Their behaviour was microscopically explained by observing concentrated suspensions. A qualitative explanation is the following.
If the shear rate is low, the motion of the particles is slow, and the liquid phase could fill all the voids between particles. In this conditions the liquid acts as a lubricant for the motion of the particles and the friction between them is low, hence the resulting stress is small.
If we increase the strain rate, the fluid dilates and the liquid is not enough to lubricate all the solid particles. This originates a solid-solid friction that increases the shear stress. To conclude we can see that this effect leads to an increasing of the apparent viscosity.
In figure 1.5 we show an example for this behaviour: experimental data for TiO_2 suspensions. As we can see, the behaviour of the TiO_2 suspension, changes in function of the concentration. In this graph the Newtonian curves are presented to compare the two behaviours. For higher volume fractions of TiO_2 we observe a marked shear thickening behaviour while for the lower (12%) we do not see any difference with the Newtonian behaviour.
Shear thickening fluids are well described by the power law model presented in equation 1.3, but in this case it is not possible to say if a limit value for the viscosity (η_0 or η_∞) exists or not [16].

Visco-plastic fluids The last class of time-independent fluids includes the visco-plastic ones. These fluids are characterized by the yield stress σ_0, i.e. a threshold value for the shear stress. If we want the fluid to flow or to deform, σ_0 must be exceeded, otherwise it would deform like an elastic solid.
The visco-plastic fluid above the yield stress could behave as a Newtonian fluid or as a shear thinning fluid (i.e. the apparent viscosity η could be constant or it could decrease with the shear rate increasing). If the viscosity above the yield stress assumes a constant value, then the fluid is called a *Bingham* fluid, otherwise, if the fluid shows a shear thinning behaviour above the yield stress, it is called a *yield pseudoplastic* fluid.
To explain the behaviour of these fluids we can give the following microscopical description. The material has a great resistance given by its rigid structures that could sustain a low stress, hence

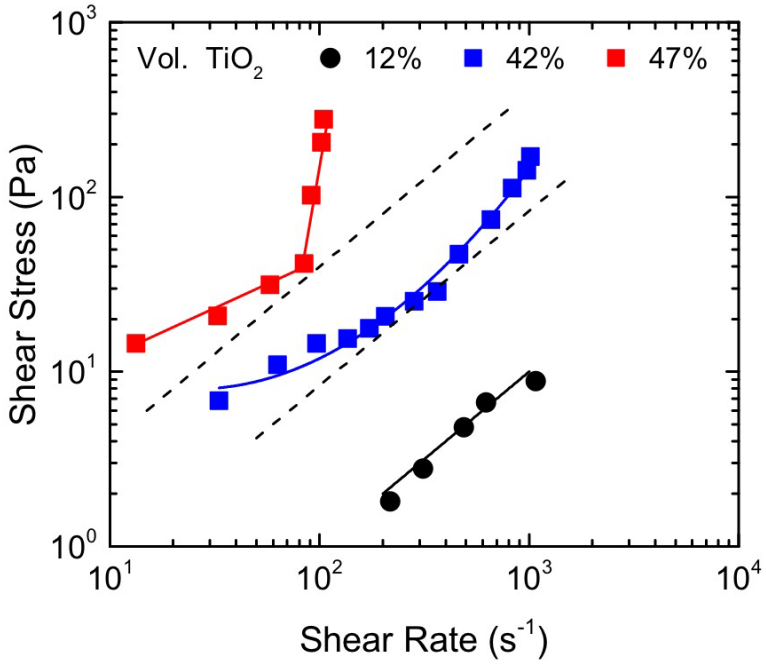

Figure 1.5 : Shear stress vs shear rate curves for TiO_2 suspensions (dots) compared with Newtonian curves (lines). Picture is taken from [16]

it might deform elastically if the applied stress is less than σ_0. If the stress overcomes σ_0, then it could break the inner structures and the material obtains a viscous behaviour. Many materials such us emulsions, foams and gels show the existence of a yield stress [21], and they are widely used in different sectors like food, pharmaceutical and healthcare [22]. For this reason the study of the yield stress is interesting for many contexts and there are several models to describe this kind of fluids. Bingham fluids are described by the **Bingham** model in equations 1.7.

$$\begin{aligned} \dot{\gamma} &= 0 && \text{if} \quad |\sigma| < |\sigma_0| \\ \sigma &= \sigma_0 + \eta_B \dot{\gamma} && \text{if} \quad |\sigma| > |\sigma_0| \end{aligned} \tag{1.7}$$

Yield pseudoplastic fluids cold be described by the **Herschel-Bulkley** model given by the equations 1.8

$$\begin{aligned} \dot{\gamma} &= 0 && \text{if} \quad |\sigma| < |\sigma_0| \\ \sigma &= \sigma_0 + m(\dot{\gamma})^n && \text{if} \quad |\sigma| > |\sigma_0| \end{aligned} \tag{1.8}$$

Another model introduced to describe the blood flow and then adapted for other viscoplastic fluids, is called **Casson** model. It is given by the equations 1.9

$$\begin{aligned} \dot{\gamma} &= 0 && \text{if} \quad |\sigma| < |\sigma_0| \\ \sqrt{|\sigma|} &= \sqrt{|\sigma_0|} + \sqrt{\eta_C |\dot{\gamma}|} && \text{if} \quad |\sigma| > |\sigma_0| \end{aligned} \tag{1.9}$$

In figure 1.6 we show two example of viscoplastic fluids: a Bingham fluid and yield pseudoplastic fluid.

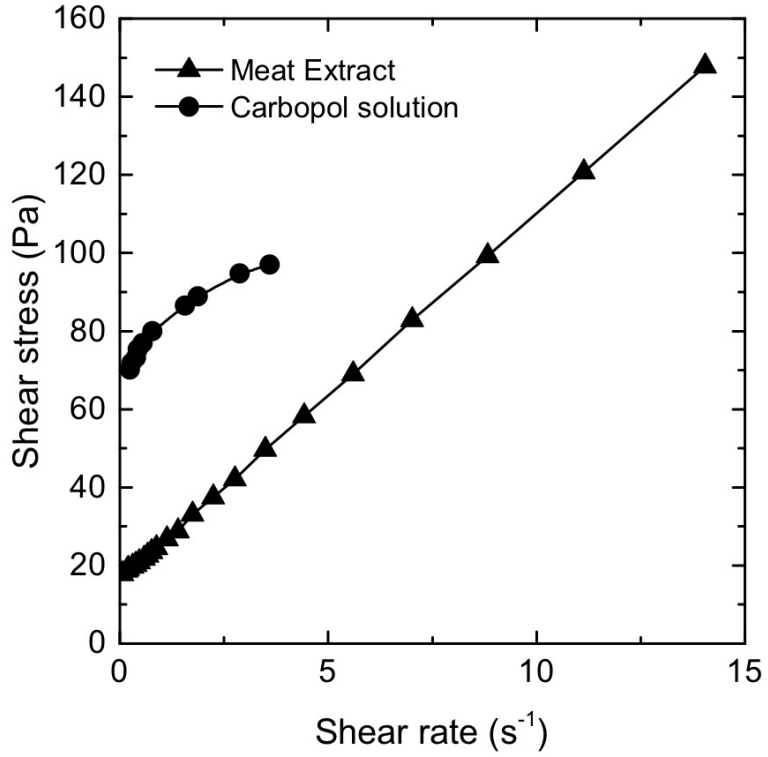

Figure 1.6 : Comparison between the shear stress vs shear rate curves for a Bingham fluid (meat extract) and a viscoplstic fluid (carbopol solution). The picture is adapeted from [16].

Now we focus on the other two classes of non-Newtonian fluids: time-dependent and viscoelastic fluids.

§ 1.2.2. Time-dependent fluids

This class of materials includes fluids that are not described by eq. 1.2. In fact the apparent viscosity obtained for these materials depends on the kinematic history. If a shear stress is applied on these materials, this affects the fluid behaviour even after. In general, η depends on $\dot{\gamma}$ and on σ as well. For example, with these materials we can see that experimental measures for the viscosity are influenced by the applied experimental procedure. We would measure different values for η in relation with the duration of the stress applying.
In general these materials could be divided into two groups: *thixotropic* and *rheopectic* fluids. A material is called thixotropic if its apparent viscosity decreases with the duration of the shearing. This behaviour could be explained microscopically, considering the material composed by inner structures that continuously brake if the shear is applied [9]. If we reduce the number of links between particles, the viscosity decreases, but at a certain point the rate of link breaking is equal to the rate of link re-building, so it is possible to reach a dynamic equilibrium.
Conversely the fluids with an apparent viscosity that increases with the duration of the shearing are called rheopectic fluids. In these systems the formation of internal structures is promoted by the imposition of a shear. For this reason the apparent viscosity for these materials increases as the shear is applied [23, 24].

In figure 1.7 we show the behaviour of these two fluids.

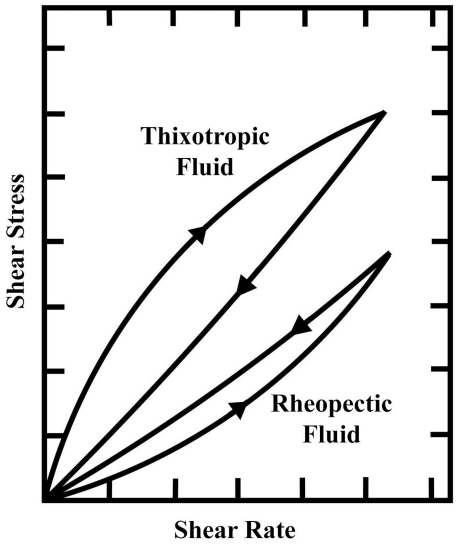

Figure 1.7 : Scheme representing the different behaviours of a thixotropic and a rheopectic fluid. The picture is adapeted from [16].

§ 1.2.3. Viscoelastic fluids

Viscoelastic fluids take this name because their behaviour is both viscous and elastic. In fact, if we consider the pure elastic configuration (Hookean solid) we could define the stress σ as a function of the strain ($\epsilon = -\frac{dx}{dy}$) and of the Young modulus G.

$$\sigma = G\epsilon \tag{1.10}$$

Otherwise, for a completely viscous fluid we could take the equation 1.1. For a viscoelastic fluid the behaviour could be described as a combination of these two equations, as we show in Maxwell equations 1.14. To obtain these equations we consider the scheme shown in figure 1.8.

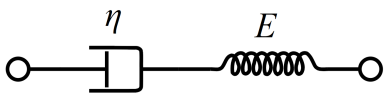

Figure 1.8 : Scheme representing the Maxwell model for viscoelastic fluids.

The fluid is presented as an elastic spring connected to a purely viscous damper. If a stress σ is applied to the system, it causes a strain $\epsilon_S = \sigma/G$ to the spring. At the same time, from eq. 1.1 we could obtain the strain for the damper just integrating

$$\eta\dot{\gamma} = \sigma \quad \Rightarrow \quad \gamma = \int \frac{\sigma}{\eta} dt + \gamma_0 = \sigma\frac{t}{\eta} + \gamma_0 \tag{1.11}$$

We could obtain the total deformation of the fluid as the sum of viscous and elastic contribution: $\epsilon_{tot} = \gamma + \epsilon_S$.

$$\epsilon_{tot} = \frac{\sigma}{G} + \sigma\frac{t}{\eta} = \sigma(\frac{1}{G} + \frac{t}{\eta}) \tag{1.12}$$

Now if we differentiate $\epsilon_{tot} = \gamma + \epsilon_S$ we obtain:

$$\dot{\epsilon}_{tot} = \dot{\gamma} + \dot{\epsilon}_S \tag{1.13}$$

and by substitution we obtain the Maxwell equation.

$$\dot{\epsilon}_{tot} = \frac{\sigma}{\eta} + \frac{1}{G}\dot{\sigma} \tag{1.14}$$

We can study this system in relation with the relaxation time $\lambda = \eta/G$. In this configuration, if the time scale of an event is short with respect to the typical relaxation time, the fluid behaves like a solid. If time scales are longer, then the fluid behaves as a viscous liquid. Another interesting feature is that, if we apply a shearing motion to this class of fluids, we obtain a stress orientated orthogonally with respect to the direction of the shear [18].
Some examples for this class of fluids are given by foams, gels, emulsions and polymeric melts and solutions.

§ 1.3. Yield stress fluids

Soft materials are materials that can be easily deformed by thermal stresses or thermal fluctuations. Soft materials include liquids, polymers, foams, gels, colloids, granular materials, and soft biological materials. A particular category of soft materials is given by Soft Glassy Materials. These materials are characterized by a microscopically disordered structure and by an extremely slow internal dynamics. For their complex inner structure they show both liquid-like and solid-like behaviours. This dual behaviour produces interesting rheological properties, widely studied in the last years.
In section 1.2.1 we described the viscoplastic fluids as fluids characterized by a yield stress. If the applied stress is lower than the yield stress these fluids do not flow. Conversely if the yield stress is exceeded, they start to flow and the apparent viscosity could assume a constant value or could decrease as for shear-thinning fluids.
To study Soft Glassy Materials (SGMs) it is important to consider these properties. In fact SGMs mostly exhibit a yield stress, and they usually behave as a shear thinning viscoplastic fluid [7].
Some examples of materials included in the category of SGMs are given by foams, gels, pastes and concentrated emulsions and suspensions. To describe these materials we could apply the Herschel-Bulkley model described in equation 1.8.
It is important to introduce the the concept of *jamming*, since it plays a central role in the behaviour of SGMs. A material is considered to be jammed if the relaxation time for its inner structures is greater than the observation window [25]. In this situation the particles appear stuck in a fixed configuration, so the material globally acquires a yield stress.
The notion of jamming is related with the volume fraction ϕ of the inner constituents of the material.

In fact at low volume fractions we can see that the particles in the material are free to move without impediment from their neighbours, so the system is not jammed. Conversely, at high volume fractions it is impossible for the particles to avoid the other constituents of the fluid. As previously said, in these conditions the microscopic structure of the material gets stuck in a fixed configuration and the fluid loses his ability to flow, originating a yield stress. It is possible to define the critical volume fraction ϕ_c which corresponds to the random close packing of monodisperse, undeformed spheres [6]. At zero temperature the critical volume fraction is known as *jamming point* [26]. It is observed that the yield stress depend on ϕ, and it decreases from $\phi \approx 1$ to ϕ_c but it persists even below ϕ_c [27].
The fluid behaviour is influenced by the temperature and by the stress, but in this case the flow is enhanced by these parameters [1].

§ 1.3.1. Concentrated Emulsion

In this Thesis we analysed the behaviour of Soft Glassy Materials, focusing on a concentrated emulsion. Emulsion refers to a class of materials composed by a mixture of two (or more) liquids. The two liquids are immiscible, and one liquid must be dispersed into the other. Hence we will distinguish them as dispersed phase and continuous phase respectively.
Emulsions are widely diffused in many fields: they are involved with the everyday life, but also with specific applications. For example we can frequently find them in food products or in pharmaceutical, cosmetics and personal hygiene products, but contemporaneously we can use them as fire-fighting agents, or we can find them in agriculture or industries applications.

Figure 1.9 : Examples of emulsions for common or for specific applications. From left to right we can see examples of food products, cosmetics, paints, fertilizers and lubricants.

If we want to categorize an emulsion is necessary to define the composing elements, i.e. the continuous and the dispersed phases. When we refer to a specific emulsion, we use the following rule: the first letter represents the dispersed phase, while the second one represents the continuous phase. For example with "O/W" we mean the oil in water emulsion, while with "W/O" we call the inverted emulsion of water in oil [28]. The emulsion preparation is called *emulsification* and it consists of dispersing one fluid into another via creation of an interface between them. This process requires energy, and the originated system is in metastable equilibrium. In fact the thermodynamic stability is reached when the system has two separated continuous phases [29]. To avoid the phase-separation,

some molecules called surfactants are introduced. These molecules are *amphiphilic* i.e. they show both hydrophilic and lipophilic properties, which means that they easily bound with both the water and the oil molecules. By introducing the surfactants it is possible to lower the surface tension between the two fluids, that traduces in a minor effort to create droplets. Moreover the surfactants cover the surface between oil and water, preventing the coalescence of droplets and leading to a more stable mixture.

Surfactants could increase the lifetime of an emulsion from a few days to years. Studies show that the surfactant should be more soluble in the continuous phase if we want to increase the stability of the emulsion [28]. The volume fraction of the dispersed phase with respect to the total is a key parameter. For emulsions this quantity could be enhanced until we reach very high values (more than 99.95%). For this feature emulsions are different from other materials, since their droplets can deform and take almost all the available voids. Another important parameter is the size of the droplets: it may change from 500 nm to a few hundred of microns. We also consider the polydispersity of the fluid, that describes how the size of droplets may change in the emulsion.

§ 1.4. Physics of fluids at the microscale

The physics of fluids at the microscale is very different from the "macrofluidics", since some negligible factors for the macroscopic scale became very important at the microscopic scale. The study of the behaviours of fluids at these scales is called microfluidics, and the considered systems usually show at least one dimension smaller than 1 mm. Some factors as surface tension, energy dissipation, and the resistance of the fluid play a central role at this scale, and they start to dominate the system. These properties originate very different behaviours for the microscale with respect to the macroscopic scale. The microscale shows some ordered behaviours that allow us to describe these systems with the classical mechanics. For example at the macroscale we usually observe the turbulent (and then disordered) flow, this needs a different kind of description if compared with the laminar (and ordered) flow easily observed at the microscale [30].

§ 1.4.1. Microfluidics

To describe the behaviour of fluids at the microscale, we need to introduce some assumptions necessary for the validity of equations that rule this kind of systems. First of all we introduce the continuum assumption: we need to study systems big enough to neglect the molecular nature of the fluid. For this reason we assume the typical size of the system to be much bigger than the "fluid particle" i.e. the volume necessary to consider a uniform density. Moreover we need to consider the fluid as incompressible i.e. the density ρ does not change under the effect of the pressure. This assumption is generically reasonable for all aqueous solutions [30]. By the introduction of these assumptions, and by considering the mass conservation principle, we could obtain the continuity equation

$$\frac{\partial \rho}{\partial t} + \nabla \cdot (\rho \mathbf{u}) = 0 \tag{1.15}$$

where ρ is the density and $\mathbf{u}$ is the velocity vector. The physical meaning of this equation is that the fluid mass flowing out from a volume V is always equal to the mass that flows into the volume in the same period of time. This means that, in a fixed volume, there is no mass variation.
If we define the external force acting on the fluid as $\mathbf{F}_{ext}$ and the stress tensor as $\overline{\overline{\sigma}}$, by applying the Newton's second law of motion to a small block of fluid we could describe the velocity field

$$\rho \left(\frac{\partial \mathbf{u}}{\partial t} + \mathbf{u} \cdot \nabla \mathbf{u} \right) = \mathbf{F}_{ext} + \nabla \cdot \overline{\overline{\sigma}} \tag{1.16}$$

Now we define the pressure gradient as ∇p and the fluid viscosity as η. If the stress is linearly related to the deformation, as for Newtonian fluids, then we could obtain a general equation describing the fluid behaviour, called **Navier-Stokes** equation

This is a vectorial equation, which means that we have three unknowns ($\mathbf{u}$), combined with the continuity equation 1.15 yield four equations in four unknowns. The Navier-Stokes equations are widely used for many applications, but the analytical solution (if it exists) is still missing. If we want to obtain the velocity field for a fluid, then it is necessary to impose some boundary conditions and some approximations that allows us to get a specific solution of this equation. For example we can

see that in some conditions the eq. 1.17 becomes the **Stokes** equation

$$\rho\left(\frac{\partial \mathbf{u}}{\partial t} + \mathbf{u}\cdot\nabla\mathbf{u}\right) = -\nabla p + \eta\nabla^2\mathbf{u} + \mathbf{F}_{ext} \tag{1.17}$$

The second therm in the left side of the equation is the inertial contribution of the fluid, and in some conditions it could be neglected. In particular, at small scales the viscous effects (second term on the right) are preponderant with respect to the inertial term.
To estimate these conditions the *Reynolds number Re* is introduced. This number represents the ratio between the inertial and the viscous contributes in the fluid's behaviour, and it is defined on typical values for the fluid and for the system: the viscosity η, the density ρ, the typical length for the system l and the magnitude of the velocity u. With these quantities we define the Reynolds number

$$Re = \frac{\rho u l}{\eta} \tag{1.18}$$

At small scales the Reynolds number is small ($Re \ll 1$), and the inertial term $\mathbf{u}\cdot\nabla\mathbf{u}$ could be neglected. In these conditions we obtain the Stokes equation 1.19 that is linear and easier to solve.

$$\nabla p = \eta\nabla^2\mathbf{u} + \mathbf{F}_{ext} \tag{1.19}$$

The eq. 1.19 has interesting solutions, in particular it is not characterized by turbulence and the solutions could be reversed, i.e. if we apply a force and then the same force is applied in the opposite direction, we would return to the initial configuration. In figure 1.10 we report the different flows observed by Osborne Reynolds with the increasing of the fluid velocity (the third sketch represents the turbulent flow observed enlightening the tube with an electric spark).

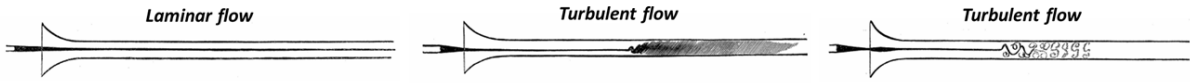

Figure 1.10 : Different flow regimes for water flowing in a pipe observed by O. Reynolds in 1883 [31]

To identify the distinction between different regimes we report some values for the fluid flow in a pipe [32]

- Laminar regime: $Re < 2300$
- Transition regime: $2300 < Re < 4000$
- Turbulent regime: $Re > 4000$.

§ 1.4.2. Parallel plates flow

We could obtain solutions for the Navier-Stokes equations 1.17 only for specific cases. One interesting configuration that could lead to particular solutions is the flow between two parallel plates.
This configuration, schematized in figure 1.11, is useful for this thesis. In fact our microfluidic channels are well described by this approximation. We will consider two infinite parallel plates with a fixed distance h.

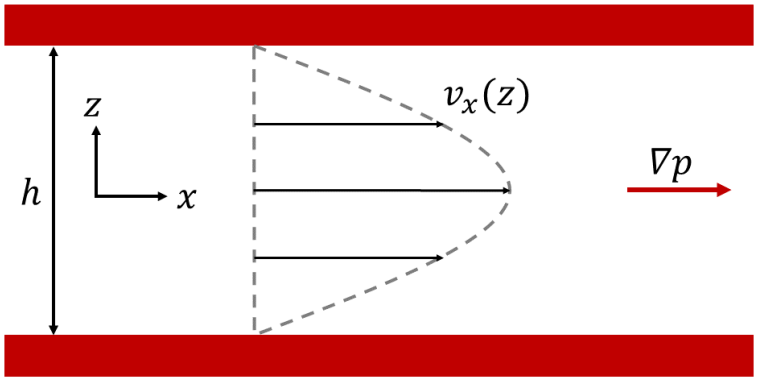

Figure 1.11 : Scheme representing the parallel plates flow. The represented velocity has the typical profile for a Newtonian fluid.

This configuration simplify the equations. Considering the laminar flow for low Re, and defining x as the channel longitudinal direction and z as the traverse direction, we obtain that the velocity has only one component different from zero: $\mathbf{u} = (u_x(z), 0, 0)$.
In these conditions the Stokes equation 1.19 becomes

$$\frac{\partial p}{\partial x} = \eta \left(\frac{\partial^2 u_x}{\partial x^2} + \frac{\partial^2 u_x}{\partial y^2} + \frac{\partial^2 u_x}{\partial z^2} \right) \tag{1.20}$$

We observe that the infinite geometry considered leads to the absence of variations along x and y, so that the only non null derivative (for the velocity) is $\dfrac{\partial u_x}{\partial z}$.
We conclude that, applying all the assumptions of incompressible Newtonian fluid in a laminar flow, the Navier-Stokes equations simplifies to

$$\frac{\partial p}{\partial x} = \eta \left(\frac{\partial^2 u_x}{\partial z^2} \right) \tag{1.21}$$

At this point it is possible to solve this differential equation, obtaining

$$\frac{\partial p}{\partial x} z = \eta \left(\frac{\partial u_x}{\partial z} \right) + C \tag{1.22}$$

With C a constant value obtained by the integration. Solving this equation applying the no-slip boundary conditions ($u_x(z = \pm h/2) = 0$) we obtain the final solution for the velocity:

$$u_x(z) = \frac{1}{2\eta}\frac{\partial p}{\partial x}\left(z^2 - \frac{h^2}{4}\right) \tag{1.23}$$

From this equation we see that the velocity profile has a parabolic shape along the height of the channel. This means, as expected, that the velocity maximum occurs in the center of the channel. From equation 1.22 it is possible to obtain the stress for a Newtonian fluid. In fact $\frac{\partial u_x}{\partial z} = \dot{\gamma}$. Remembering eq. 1.1 we finally obtain

$$\sigma = \frac{\partial p}{\partial x} z \tag{1.24}$$

In figure 1.12 we show the obtained profiles for velocity and stress for the flow of a Newtonian fluid between parallel plates.

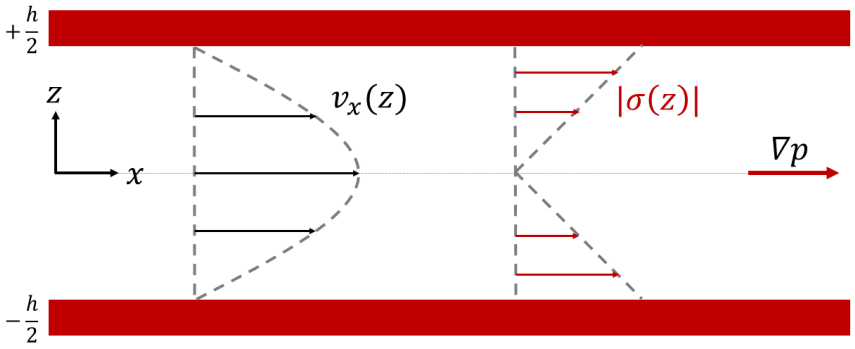

Figure 1.12 : Scheme representing the velocity and the stress profiles in function of z for a Newtonian fluid.

§ 1.4.3. Yield stress fluids flow

Now we describe the flow of Yield stress fluids in microfluidic channels. Their behaviour is useful for the description of SGMs. In particular we study the flow in the parallel plates configuration for a Bingham viscoplastic fluid, i.e. the fluid described by equations 1.7. We rewrite these equations as

$$\begin{aligned} \frac{du_x}{dz} &= 0 && \text{if} \quad |\sigma| < |\sigma_0| \\ \frac{du_x}{dz} &= \frac{\sigma - \sigma_0}{\eta} && \text{if} \quad |\sigma| > |\sigma_0| \end{aligned} \tag{1.25}$$

These equations describe a fluid characterized by a yield stress σ_0, so the flow is null unless this stress is exceeded. If the fluid is affected by a stress greater than σ_0 the flow is enhanced, but we have to consider that the stress is not uniform all along the channel. For different z we have a different stress, in particular we observe a region in the center of the channel, where the stress is below σ_0. With this stress the shear is null, so the velocity profile is flat.
It is possible to calculate the size of the plug region characterized by the flat velocity profile [18]

$$z_p = \left(\frac{dp}{dx}\right)^{-1} \sigma_0 \tag{1.26}$$

Thanks to this equation we can describe the shear rate as a function of the position in the channel. The symmetry of the channel allows us to describe the flow from $z = 0$ to $z = +h/2$ neglecting the other half of the channel since it shows the same behaviour.

$$\begin{aligned} &\frac{du_x}{dz} = 0 && \text{if} \quad 0 < z < z_p \\ &\frac{du_x}{dz} = \frac{dp}{dx}\left(\frac{z - z_p}{\eta}\right) && \text{if} \quad z_p < z < +\frac{h}{2} \end{aligned} \tag{1.27}$$

It is possible to solve these differential equations, obtaining

$$\begin{aligned} &u_x(z) = C_1 = u_p && \text{if} \quad 0 < z < z_p \\ &u_x(z) = \frac{1}{\eta}\frac{dp}{dx}\left(\frac{z^2}{2} - z \cdot z_p\right) + C_2 && \text{if} \quad z_p < z < +\frac{h}{2} \end{aligned} \tag{1.28}$$

Then, we calculate the values of C_1 and C_2 by applying the boundary conditions

$$\begin{aligned} u_p &= u_x(z = z_p) \\ u_x(z = h/2) &= 0 \end{aligned} \tag{1.29}$$

And we finally obtain the velocity profile for the flow of a Bingham fluid between two parallel plates.

$$\begin{aligned} &u_x(z) = u_p = \frac{1}{2\eta}\frac{dp}{dx}\left(z_p^2 - \frac{h^2}{4}\right) + \frac{\sigma_0}{\eta}\left(z_p - \frac{h}{2}\right) && \text{if} \quad 0 < z < z_p \\ &u_x(z) = \frac{1}{2\eta}\frac{dp}{dx}\left(z^2 - \frac{h^2}{4}\right) + \frac{\sigma_0}{\eta}\left(z - \frac{h}{2}\right) && \text{if} \quad z_p < z < +\frac{h}{2} \end{aligned} \tag{1.30}$$

In figure 1.13 we show the behaviour of a Bingham fluid, showing the velocity profile from the center to the wall. We can see the plug region between $z = 0$ and $z = z_p$ where the velocity assumes a constant value, and the other region where $\frac{du_x}{dz} \neq 0$.

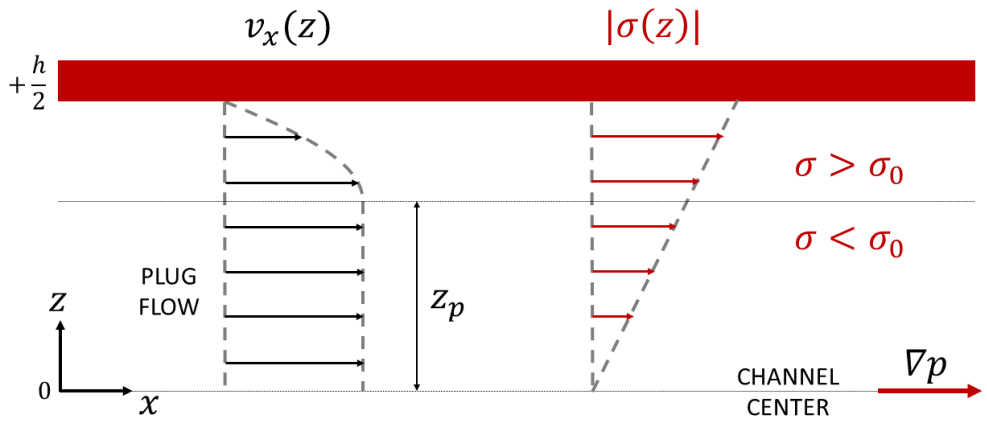

Figure 1.13 : Scheme representing the flow of a Bingham fluid between two plates. We represent only half of the channel, from the center to the top wall.

§ 1.4.4. Slip velocity for Soft Glassy Materials

The equations used to describe the flow in a parallel plate configuration (eq. 1.23, 1.30) were obtained by applying the boundary conditions. In particular we applied the no-slip boundary condition at the solidliquid interface. This condition is an assumption that cannot be derived from first principles [33] and it is not explained yet, but it has been observed expecially for Newtonian fluids at low Reynolds numbers [34, 35].
However this condition has been widely studied and the proposed explanations are usually based on frictional or viscous forces acting on the particles of the fluid and keeping them stuck on the wall.
Conversely, in a wide range of experimental studies [36–38] the observed slip velocity was greater than zero. When the slip velocity is different from zero, it is useful to keep the no-slip condition introducing the idea of slip length i.e. the distance from the wall surface to the point where the velocity profile should reach $v = 0$. This point could be estimated by observing the slip magnitude, and it could be inside of the solid if the slip velocity is greater than zero, or it could be outside if a stagnant layer is observed. In figure 1.14 we could observe some schemes for these behaviours.

The wall slip affects the non-Newtonian fluids more than the Newtonian ones.
The different behaviour is given by the more complex structure of non-Newtonian fluids, this characteristic introduces many factors that promote the wall slip, especially for multi-component fluids.
The effect of the slip depends on the fluid and on the stress. For example, for shear thickening fluids the effect of wall slip is sharpened at high shear stress, while for shear thinning it affects the flow at low stress. It is proved that the wall slip depends on various parameters. First of all it depends on the fluid properties as the existence of a yield-stress, the viscosity, or the density [39–41]. Moreover the wall slip could be influenced by the flow regime i.e. by the Reynolds number, and by the system temperature and pressure [42–44]. Finally the wall slip is widely influenced by the wall properties as

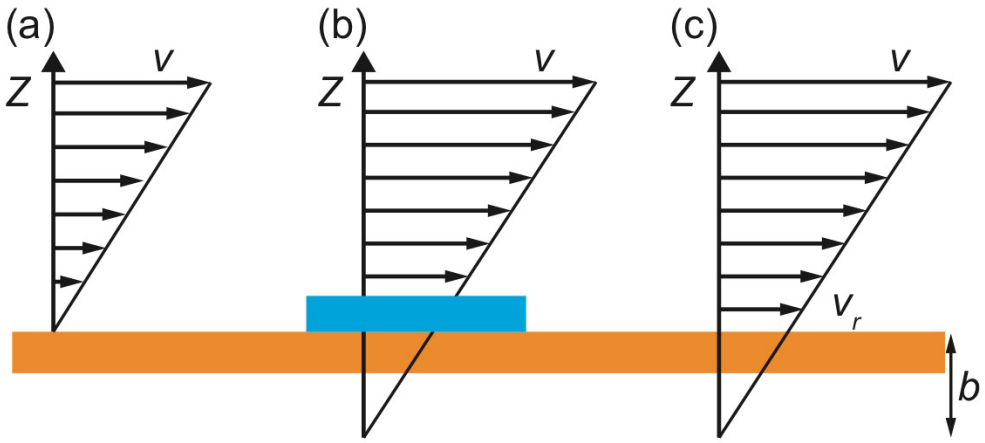

Figure 1.14 : Scheme representing the various slip conditions. (a) represents the no-slip boundary condition, while in (b) we observe a stagnant layer and in (c) we observe a partial slip length. Picture taken from [18]

wettability and roughness of the surface [12, 13, 45].
Some explanations for the wall slip phenomenon are given by [40]. The existence of a thin lubricant film between the fluid and the wall could be the cause for this behaviour. The lubricant layer could be given by different causes, for example it could be on the surface prior to the introduction of the fluid, or in an emulsion it could be originated by a layer of continuous phase from the bulk.
Moreover, in yield stress fluids, it could be generated by the applied stress, and it could lead to an apparent yield stress. If the stress affects the fluid with the creation of a thin film near to the wall, the slip could let the fluid flow, hiding the yield behaviour. This lubricating layer would be created by a local stress above the yield value on the wall, and below the yield in the rest of the channel.
In general we could distinguish between three different flow regimes of slip:

- slip at low stress, the flow is completely caused by the slip;
- stress slightly above the yield stress, the flow is given by both the slip and the bulk flow;
- stress well above the yield stress, the flow is completely influenced by the bulk deformation.

§ 1.5. Emulsion Rheology

In this thesis we study the concentrated emulsion behaviour. Emulsions have very different rheological behaviours, highly influenced by the emulsion itself. In particular, the relation between stress and strain for an emulsion depends on the emulsion properties as the composition, the size and distribution of the droplets, the interactions between droplets and between emulsion and walls.
The emulsion behaviour strongly depends on the volume fraction ϕ of the dispersed phase with respect to the total. As previously observed in section 1.3, at high volume fractions the emulsion loose its ability to flow, while a dilute emulsion flows as a viscous fluid. In particular, in figure 1.15 we show the viscosity of an emulsion in function of the volume fraction, observing different behaviours.

At low volume fractions droplets are not deformed and the viscosity is highly influenced by the continuous phase, while droplets are "just flowing" with it. When we reach the volume fraction for the

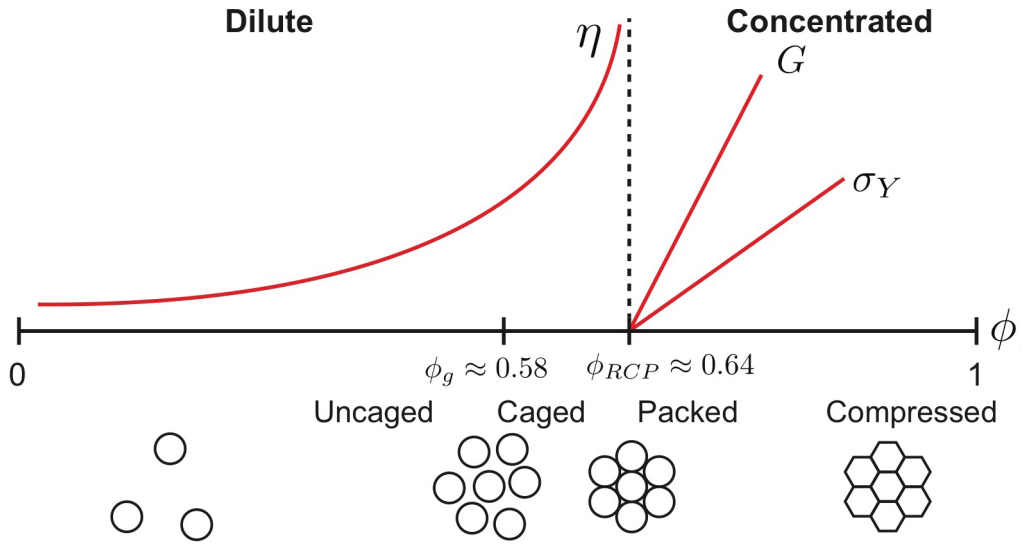

Figure 1.15 : Scheme representing the emulsion behaviour and the droplets deformations in function of the volume fraction. Figure taken from [18].

hard sphere glass transition $\phi_g = 0.58$, we obtain a caging scenario where the behaviour of a droplet is influenced by the others since they often collide. At this volume fraction the viscosity increases. When we reach the critical volume fraction $\phi_c = 0.64$ related to the random close packing, droplets are packed and they start deforming as the volume fraction is increased. The more the volume fraction is increased, the more the droplets deform, and the yield stress increases with it.

To explain this behaviour more models have been suggested and experimentally tested in years, starting from the two-dimensional hexagonal model proposed by Princen [3], and going to more complex 3D models [46, 47].

These models are based on the following considerations. When the volume fraction overcomes ϕ_c and the droplets start to deform, energy is stored in the surface between droplets. The stored energy increases with the deformation of the droplets and this deformation is elastic. In fact, if the droplet is set free, it returns to its spherical form. If we apply a sufficiently high strain, we could induce rearrangements i.e. droplets change their neighbours, and the energy stored in the deformation could be dissipated in the fluid flow.

We see that, below the yield stress the rearrangement is not allowed and there is only an elastic deformation of the structure, while above the yield stress rearrangements cause the liquid-like flow of the emulsion.

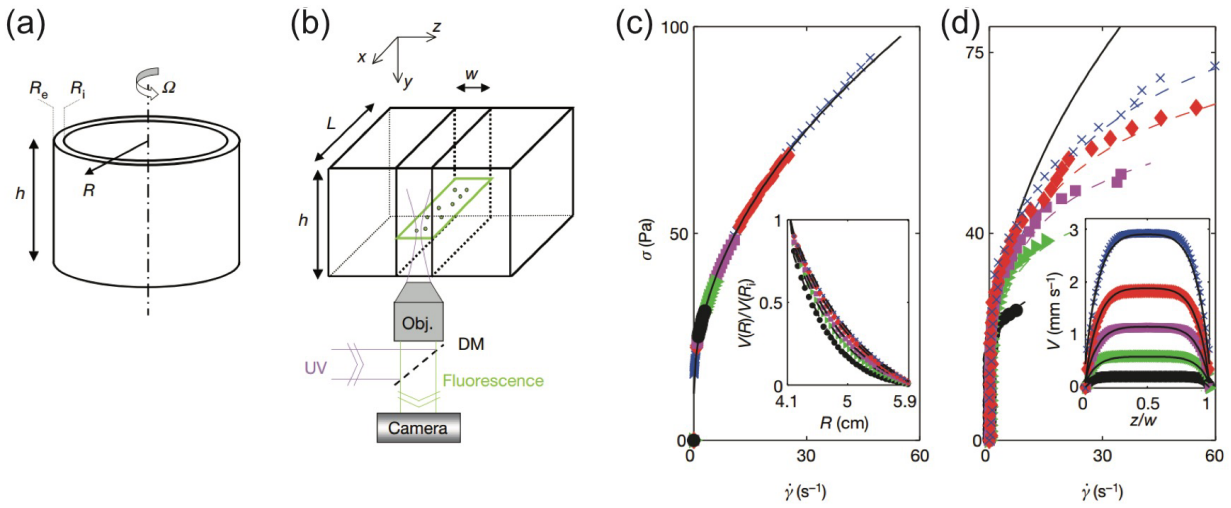

Figure 1.16 : Representetion of the Couette cell (a) and of the microfluidic channel (b) adopted in [10]. (c) and (d) are the respective flow curves. Figure reproduced from [10].

§ 1.5.1. Concentrated Emulsion Flow

The flow of a concentrated emulsion with a volume fraction $\phi > \phi_c$ was widely studied, and the yield stress was described by several models.
First of all the value of the yield stress was investigated. Mason [6] observed a dependence from the volume fraction ϕ and described the yield stress behaviour for concentrated emulsions with $\phi > \phi_c$, observing the following proportionality:

$$\sigma_0 \propto \left(\frac{\gamma}{a}\right)(\phi - \phi_c)^2 \tag{1.31}$$

with γ the surface tension and a the droplet radius.
We have already seen that the relation between stress and strain beyond the yield regime could be described with the Herschel-Bulkley model described in eq. 1.8 (i.e. $\sigma/\sigma_0 - 1 \propto \dot{\gamma}^n$). Experimental data described in [6] agree with this model, if $n = 0.5$.
Other works show that the jammed emulsion behaviour under confinement is not easy to describe, and it is very different from the bulk flow. For example, Goyon and coworkers observed a non-local behaviour by comparing the flow of concentrated emulsion under confinement conditions for two different geometries [10]. In these works, the local shear rate was compared to the local shear stress, and they observed that the local flow behaviour cannot be accounted by a single master curve (results are reported in figure 1.16).

We observe that the relation from σ and $\dot{\gamma}$ id different for different curves. Therefore, for these fluids, the viscosity changes for different conditions. Then, for a given σ the resulting γ may not be the same.
The flow is related with long range interactions, hence it cannot be described by a linear relation

between local stress and local strain. For these reason it is called non-local behaviour [48].
This behaviour is related to the fluidization of the emulsion, and it is caused by the plastic rearrangements that happen in the material when confined in microchannels [49, 50]. The rearrangement behaviour is based on the accumulation of stress through the droplet deformation. If the yield stress is exceeded, then the accumulated stress is released and it originates the rearrangements.
The cooperativity length ξ and the fluidity f are useful quantities to describe the non-local behaviour. ξ measures the extension of the non-local correlations and quantifies the spreading of the plastic activity, while $f = 1/\eta$ shows the ability of the fluid to flow. It is possible to relate ξ to f through a diffusion-relaxation equation in order to deal with non-local effects [51]. Moreover it is observed that ξ is only function of the emulsion volume fraction ϕ [10, 12].
Another interesting parameter is the rate of plastic rearrangements Γ. Studies showed that it is proportional to the fluidity i.e. $\Gamma \propto f$ [51].
Since the non-local behaviour affects the fluid flow for confined concentrated emulsions, it is interesting to study how the walls affect these flows. In fact, close to the walls surface properties can trigger rearrangements and the flow is widely influenced. The wall effect on this flow was studied in a limited number of works as [11–13, 49]. In particular in [11] they studied the flow of concentrated emulsions in micro-channels. The walls of these channels were decorated with pillars, and the study was performed on the effects of the pillars height. They observed that the height affects the wall fluidization in a non-monotonous way. In fact the enhancement on the fluidization depended on the different rate of platic rearrangements, and this is not in a linear relation with the pillars height. On the other hand, Paredes [49] showed the effects of the walls wetting properties on the fluid flow. In this case the cooperativity length is influenced by the plastic rearrangements induced by droplets absorbed and fixed on the wall.
Other works [12, 13] studied the flow of concentrated emulsion in microfluidic channels, observing the effects of the wall roughness on the flow. In particulare they studied different roughness shapes, changing the grooves gap g and width w. In [12] they compared smooth walls and rough walls, observing that the rate of rearrangements is enhanced by the number of grooves. This leads to the fluidization of the fluid, that results in profiles more liquid-like for the rough wall. The periodicity of the grooves influences the flow, a low periodicity generally leads to less rearrangements.
In [13] they observed two different behaviours in function of the grooves gap: for a wide gap ($g \gtrsim 3$ droplet diameters) the emulsion droplets are just influenced by obstacles, enhancing the fluidization, while for a narrow gap ($g \lesssim 3$ droplet diameters) the droplet is trapped in the gap and it becomes a "soft-obstacle" for the other droplets. In figure 1.17 we show these two behaviours.

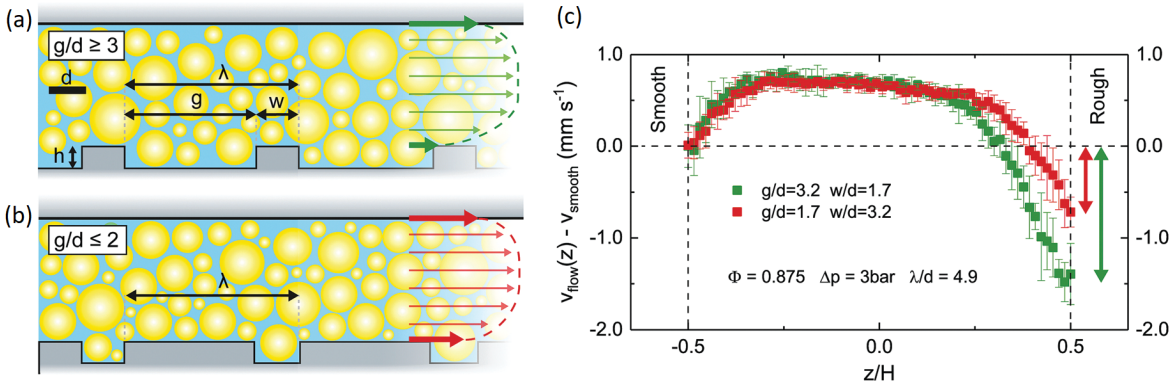

Figure 1.17 : Representetion of the wall roughness effect on the flow of concentrated emulsion. (a) and (b) shows the two different scenarios observed, respectively wide and narrow gaps. In (c) are reported the velocity profiles for these two behviours. Figure reproduced from [13].

Chapter 2

Materials and Methods

In this chapter we describe the emulsion (section 2.1), the microfluidic channels (section 2.2), and the procedure to measure the velocity profiles (section 2.3).
First of all in section 2.1 we describe how the emulsion used for our experiments was prepared, then, in subsection 2.1.1 we focus on its microscopical properties describing how they were measured.
In section 2.2 the microfluidic channels are described, reporting their fabrication parameters 2.2.1 and the procedure to follow to obtain working channels 2.2.2. In section 2.3 we describe the micro Particle Tracking Velocimetry set-up (subsection 2.3.1) and the experimental procedure (subsection **??**). Finally, in subsection 2.3.3 the analysis for collected data is described.

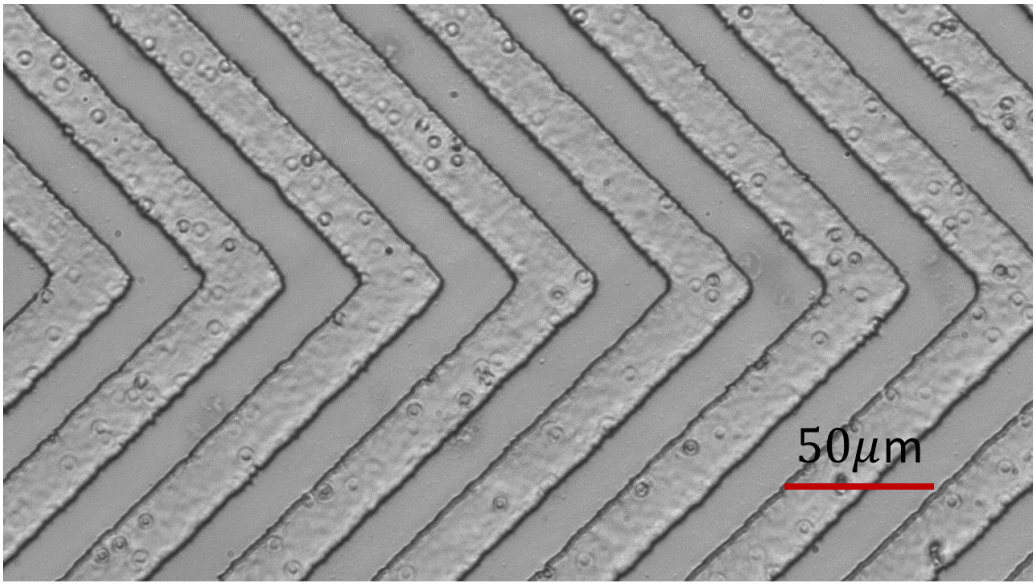

Figure 2.1 : The roughness on the wall of a microfluidic channel. Picture taken with the experimental setup described in section 2.3, with a 60× magnification.

§ 2.1. Preparation of concentrated emulsion

The process of emulsification is well known, and it is described in many works [52–54]. The batch of oil-in water emulsions used in this thesis has been originally produced in the LaFSI lab, and it was composed as follows.
Dispersed phase (droplets):

- Silicone oil (Rhodosil 47 v 1000, Bluestar Silicones, France)

Continuous phase:

- distilled water
- glycerol (Sigma-Aldritch, Germany)
- surfactant (Tetradecyltrimethyl-ammonium bromide $C_{17}H_{38}N^{+}Br^{+}$ also called TTAB)
- fluorescent tracers (Fluospheres®carboxylate modified microspheres, size $d \sim 0.2\ \mu m$)

First, water and glycerol have been mixed to obtain the liquid continuous phase. In order to reduce scattering or other optical distortions during image acquisition, the refractive index of the continuous phase was adapted to match the refractive index of the silicone oil. This allowed us to finally get a transparent emulsion. To match the refractive indexes, glycerine and water were combined at 54%(w/w). Then the surfactants and the tracer were added at 1%(w/w) and 0.002w/w% respectively. At this point, the silicone oil was added gradually ($\sim$ 1ml/min)in order to create the droplets. The oil was added until an extremely high volume fraction was reached. Usually, the final volume fraction of the oil droplets respect to the total was about $\phi = 0.93$.
After that the emulsion was diluted adding the same liquid of the continuous phase, until a volume fraction $\phi = 0.875$ was reached. This was done to obtain a more stable emulsion because, if the volume fraction is too high, the emulsion is unstable and droplets start coalescing.
Finally, all the produced emulsion ($\sim 300\ ml$) was stored in centrifuge tubes of about 50 ml.
When needed for experiment sessions, the emulsion was diluted at the selected volume fraction by adding a controlled amount of continuous phase, and then centrifuged to remove the air bubbles stored during the mixing. The centrifugation process is necessary because air bubbles could affect the number of rearrangements, and this is the only reliable method to remove them.

Figure 2.2 : Diluted emulsion in a becher, before being stored in syringes for experiments.

§ 2.1.1. Emulsion characterization

It is of fundamental importance to determine size and size distribution of the droplets of the emulsion. To this aim we imaged the emulsions and we used specific software for object recognition. To obtain separated droplets we diluted the emulsion in aqueous solution of 1% TTAB since TTAB helps to keep the silicone oil in dispersed phase. Once obtained this solution, we placed a few drops of this solution between two microscope coverslips. We took some images under bright field optical microscope with a 100× magnification objective, as showed in Figure 2.3. Then, the size of the droplets was determined with NIS Elements, the software related to the microscope that allows us to obtain the dimension of objects in figures, thanks to a specific calibration for every objective.
We measured $\sim$ 400 droplets saving the values of each diameter. Measured values were averaged over several hundreds of droplets and the mean droplet diameter $\langle d \rangle$ was determined. Moreover, we calculated the polydispersity index defined as the coefficient of variance: $C.V. = \sqrt{Var(d)}/d \times 100\%$. Final results are $\langle d \rangle = 8.9\ \mu m$, $C.V. = 51\%$.

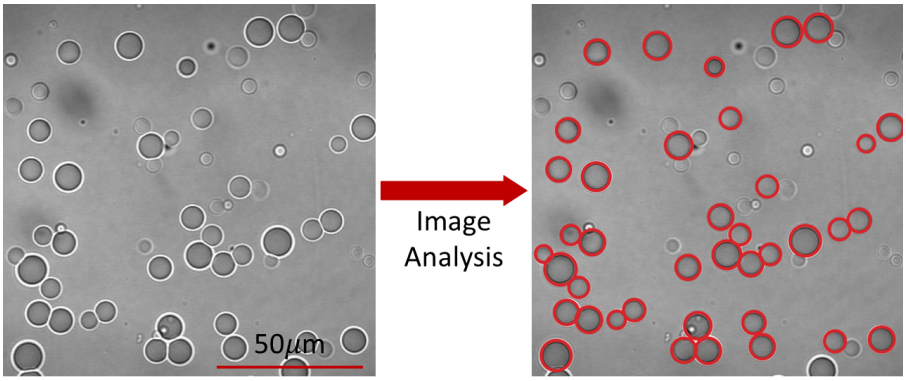

Figure 2.3 : Example of the droplet size analysis. We can see an original image obtained with the microscope, compared with the analysed image.

The emulsion was tested in [18] to check the stability of the droplets. To do that they measured repeatedly the diameter of the droplets in different moments: as soon as the emulsion was produced and within a 2-months period. Moreover the droplet size was measured either before or after it flew into the microfluidic channels to see if the flow could affect the droplets. In all these measures no noticeable difference was observed between the droplets.

§ 2.2. Microfluidic Channels

To assess the role of the wall roughness we need to pattern the channels walls with microstructure having length scale comparable to the emulsion droplets. Within our facilities it was not possible to obtain resolutions of a few microns as the ones required in [13] ($d \sim 5\ \mu m$).
For this reason the channels were realised by standard multilayer UV photolithography equipped with a mask aligner, at the Institute of Physical Chemistry, Polish Academy of Science (IPC, Warsaw, Poland) in the group of Prof. Piotr Garstecki.
The roughness was shaped with two different geometries. First of all rectangular grooves were made, perpendicular to the flow direction. Several geometries have been realised, from the herringbone structures to straight grooves perpendicular to the flow direction.

§ 2.2.1. Grooves layout

In figure 2.4 we can see the different topologies of grooves used in this thesis. In particular, figure (a) represents the straight grooves, i.e. a succession of equally spaced rectangular posts (the spacing gap is called g), with a fixed height h and width w. The period of these grooves is called $\lambda = g + w$.
Different channels were fabricated, with several combinations of g and w, but for this thesis we only used the channel with $g = 15\ \mu$m, $w = 15\ \mu$m.

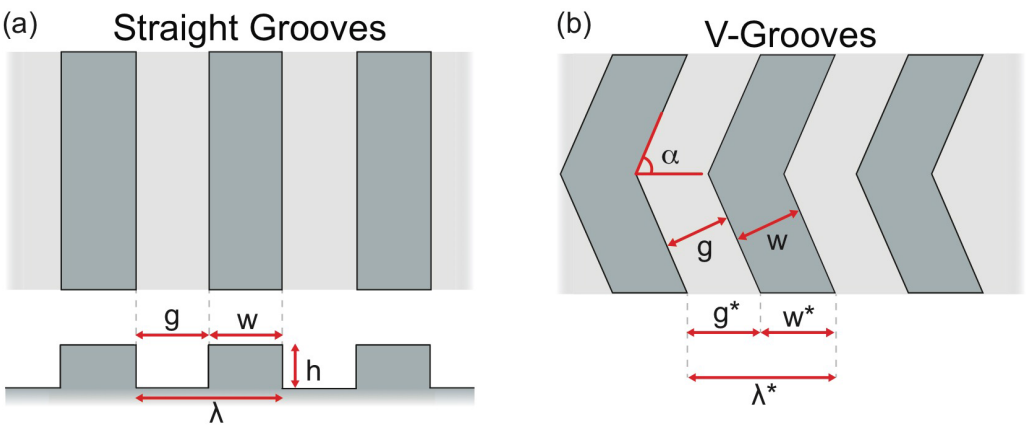

Figure 2.4 : Schemes representing the different groove layouts. In figure (a) we can see straight grooves, while in figure (b) are represented herringbone grooves. Pictures taken from [18].

In figure 2.4(b) we show the herringbone grooves. The tips of the herringbone grooves coincide with the longitudinal axis of the channel. We define α the angle between the groove and the channel longitudinal axis. We point out that, in this case of herringbone grooves, we need to consider also the projection of g and w on the flow direction. These quantities represent the effective gap and width for tilted grooves, and we call them respectively g^*, w^*. Similarly, we define an effective $\lambda^* = g* + w*$.
For this thesis we investigated different angles ($\alpha = 30°,\ 45°$) with different g and w. In Table 2.1 we summarize the patterns adopted for our experiments.

α [deg]	w-g combination [μm-μm]	w^*-g^* combination [μm-μm]
30	4-4	8-8
30	7.5-7.5	15-15
30	12.5-12.5	25-25
45	8-8	11.3-11.3
45	10.6-10.6	15-15
90	15-15	15-15

Table 2.1 : List of the channels used for experiments in relation with their roughness

Roughness characterization The roughness characterization has been performed at the IPC (Warsaw) with an optical profilometer (SENSOFAR S neox, Spain), that allowed us to obtain a 3D surface topography of a large area in few seconds with a resolution up to up to 0.2 μm (magnification of 50×).
By a detailed analysis of the optical profiles we estimated a reproducibility within 1%. Grooves looked well structured with sharp edges and the surfaces have a mean roughness (RMS) of 150 nm (negligible if compared to the grooves height of $\sim$ 2.5 μm). Fluctuations were reported in the channel height, due to fabrication imperfections. These fluctuation are always below 5%.

§ 2.2.2. Channel preparation

In this thesis we realized microfluidic channels using the patterned surfaces obtained in Warsaw. To flow the emulsion, it was necessary to combine a flat surface of the channel to the patterned one. One of the surfaces had to be drilled, in order to apply two tubes to make the emulsion flow.
First, we drilled a microscope slide to create holes for the tubes. The slide was then cleaned with isopropanol and used as the second surface of the channel, opposed to the patterned one. To seal the two surfaces, we needed to put a glue between them, keeping a fixed height. In our case, the best solution was using a dry film photoresist instead of using a glue. In fact, the dry photoresist used (WBR-2000 produced by DuPont, USA) has a fixed height of 120 μm, so it is enough to put this film between the two plates to obtain a closed channel with a fixed height.
To this aim, we used a knife plotter (Craft Robo CC200-20, Graphtec, Japan) to cut the channel shape in the photoresist. Later, the dry film photoresist was disposed on the plate with the roughness. It was important to keep the rough region inside the channel shape and press the photoresist in order to remove the trapped air bubbles. After that the cover plate was disposed on the photoresist, and the channel was closed. Therefore it still needed to be put under hydraulic press for 5 minutes at 80° C with a pressure of 2 bar, in order to obtain a better adherence between the surfaces. Finally, the channel was exposed to UV light (i-line 365 nm) for 60 seconds. This part of the process was necessary to polymerize the photoresist, in order to harden the film between the two plates.
With this procedures we obtained a microfluidic channel with height $H = 120$ μm, length $L = 45$ mm and width $W = 4$ mm. At this point two syringe needles were glued to the channel holes with commercial glue.

Surface modification Before using channels for experiments, another step was necessary. Several studies [18] observed that the emulsion easily coalesces when it flows inside the microfluidic channel. They observed that this phenomenon took place either for glass and resist surfaces, and they noticed that the different wetting properties of the materials could strongly influence the slip velocity. For these reasons channels were treated with a non-ionic hydrophilic coating. The coating was produced with water and PVP (Polyvinylpyrrolidone K90, AppliChem). The channel was treated with a oxygen plasma to activate the inner surfaces and then the water-PVP solution (2.5% w/w) was fluxed inside the channel for 2 hours with a syringe pump. The flow rate was $\sim$ 3 (ml/h). The effectiveness of this treatments is verified with contact angle measurements, and during measurements we could qualitatively see the difference between a treated channel and an untreated one.

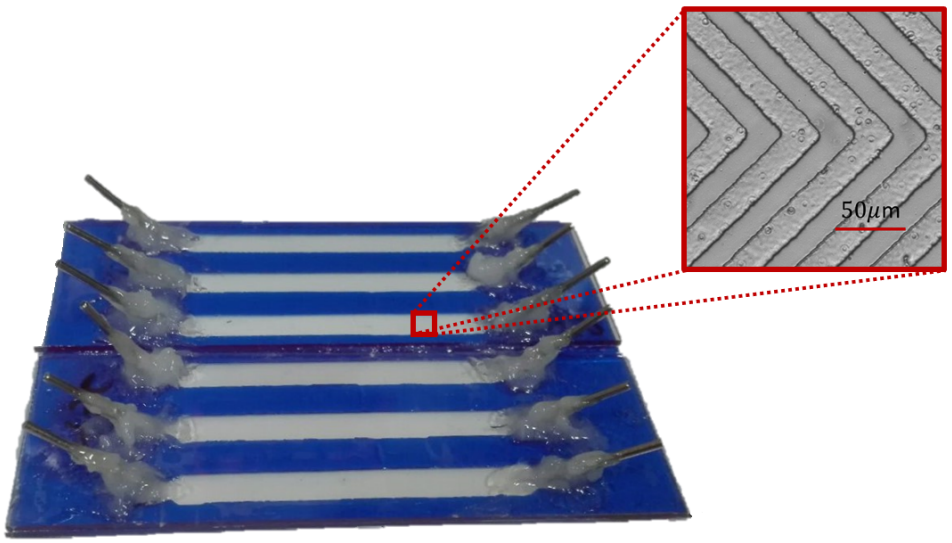

Figure 2.5 : A sample of six microfluidic channels ready for the measurements.

§ 2.3. micro-Particle Tracking Velocimetry: experimental setup and data analysis

To measure the flow profiles in microfluidic channels, we used the micro-particle tracking velocimetry (μPTV) technique. In this section we describe the experimental setup used to collect data and the procedure to analyze them.

§ 2.3.1. Experimental Setup

Emulsion flow The emulsion flow was induced by a pressure drop Δp applied on the emulsion reservoir by a microfluidic pressure controller (OB1 Mk3, Elveflow, France). This device was connected to the computer and it was possible to choose a pressure drop from 0 bar to 8 bar. The pressure controller measured the difference of pressure between the channel inlet and outlet and automatically tuned the provided pressure drop. This allowed us to obtain a pressure control with an error of 0.1%. Two teflon tubes connected the emulsion reservoir to the channel and then to the emulsion bin. To keep controlled the fluid resistance, these tubes have always a fixed length $L_{tubes} = 28.0 \pm 0.3$cm.

Acquisition As described in section 2.1, we introduced in the continuous phase dye tracers labeled with Rhodamine B ($\lambda_{excitation} \sim 540$ nm, $\lambda_{emission} \sim 560$ nm). Tracers are imaged by an optical inverted microscope (Eclipse Ti-E, Nikon, Japan) using a Laser illumination(Reutner, DPSS, $P_{max} = 100$ mW, Austria) in the epifluorescence configuration (figure 2.6). Conversely, emulsion on the walls and alignment procedures have been done in bright illumination.

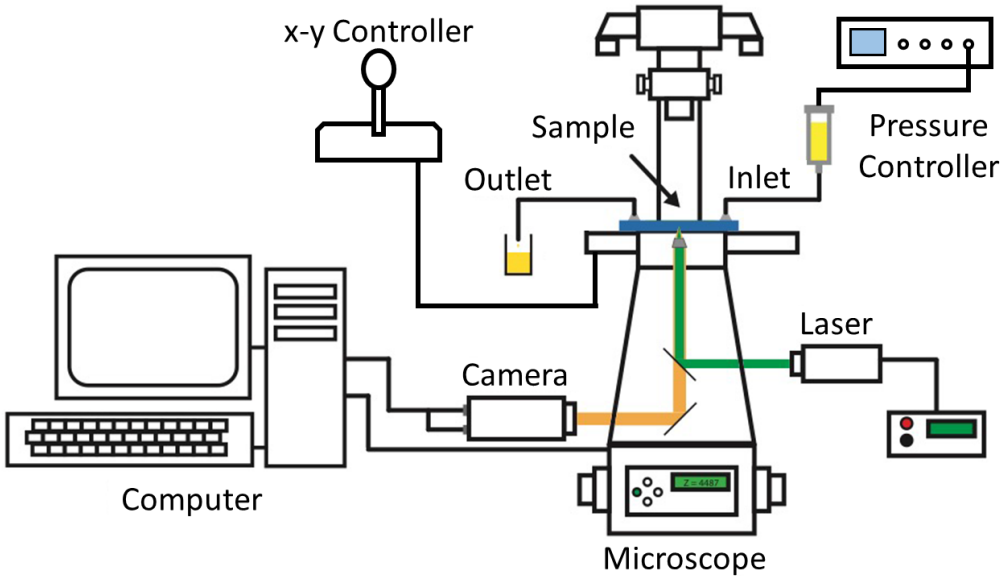

Figure 2.6 : Scheme of the experimental setup adopted for our measures. Picture adapted from [18]

To record the emulsion flow we coupled the motorized z-stage of the inverted microscope to a sCMOS camera (Zyla 5.5, Andor, UK). The sample to analyse is irradiated by a DPSS laser beam with wavelength $\lambda_{excitation} = 532$ nm.
We set up an epiluminescence microscopy configuration: the excitation light is reflected on the sample

(emulsion) by a dichroic mirror (TRITC band-pass emission filter, spectral bandwidth 570−620 nm) through the objective lens. Therefore, in this configuration the objective is used to illuminate the sample at the excitation band and collect the light emitted in the emission band at the same time.
The objective used for the measures was a 60×, apochromatic corrected, long working distance ($WD =$ 2 mm) objective, with a numerical aperture $NA = 0.7$ (SuperPlan Fluo, Nikon, Japan). The motorized microscope allowed us to adjust the vertical position of the objective with step resolution of 0.025 μm. The refractive index of the emulsion is $n = 1.41$, and the pixel-to-pixel spacing on the CCD sensor is $e = 10$ μm. With these parameters, the depth of field δz of the microscope objective is

$$\delta z = \frac{n\lambda_0}{NA^2} + \frac{ne}{NA \cdot M} = 1.5 \ \mu\text{m} \tag{2.1}$$

We selected a Region Of Interest (ROI) for collecting images with a resolution of 320 64 pixels. The corresponding field of view is 357 μm.

§ 2.3.2. Experimental procedure

First, the channel was set on the microscope. It was possible to move the sample on the $x-y$ plane with a motorized translation stage (Thorlabs) characterized by a sub-micrometrical resolution. We used the motorized stage to move the channel, and select the ROI with respect to the grooves. The selected positions are defined below. Then we applied a pressure drop, filling the channel and the tubes. At this point the channel was illuminated by the laser beam, and we checked the positions of the bottom and top walls. Every time that the channel was illuminated by the laser beam, the other light sources were suppressed.
Once the position was fixed and the channel was ready for the measures, we initialized the acquisition by using a custom macro. To collect a flow profile, the motorized microscopes moved the objective (focused inside the channel) over the entire channel height (H). The acquisition started from the lower wall and proceeded towards the upper surface. The objective was moved with steps $\Delta z = 2$ μm, and for every step the camera registered a fixed number of frames N_f for the μPTV.
The final result is a collection of files stored in the computer. Every file contains the N_f frames and it is related to a certain z.
Exposure time τ_{exp} and N_f were defined before every measure. τ_{exp} was defined observing the limits of the flow conditions (for a faster flow the exposure time should be shorter, otherwise the shape of the tracers recorded from the camera would elongate, and we would obtain lines instead of points). In our conditions the adopted exposure times were $\tau_{exp} = 1,\ 0.5,\ \sim 0.3$ μs. The frame rate (F.R.) was the maximum consented by the selected exposure time: respectively F.R. = 1000, 2000, 3000 fps.

In section 1.5.1 we discussed the results reported in [13] and [12]. These works show the flow of a concentrated emulsion in a microfluidic channel, and they focus on the effect induced by a rough wall. The rough wall was patterned by straight grooves, perpendicular to the flow direction, and the study shows how the flow changes with respect to these grooves. The straight grooves discussed in [13] were characterized by a symmetric roughness, for this reason the flow would have been symmetric with respect to the transversal section. In this thesis we address the effect given by a new kind of roughness.

In fact our roughness is made up by herringbone structured rectangular grooves. Therefore , in our case, the symmetry is lost due to the V-Grooves roughness, hence the asymmetric roughness gives us new effects to describe and new quantities to consider.
This asymmetric structure allows us to set a favoured direction on the herringbones patterned channel: we chose the direction given by the tips of the grooves as the main direction, as presented in Figure 2.7.

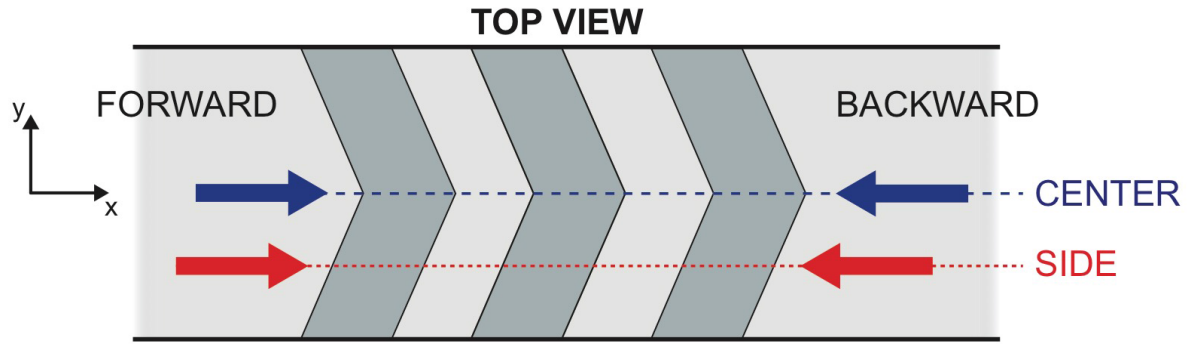

Figure 2.7 : Scheme representing the V-grooves roughness. Flow directions are indicated by arrows and labelled as *forward* and *backward*. Streamlines along y direction (transverse) are indicated by dashed and dotted lines. The long-dashed line indicates the stream at the center of the channel while the dotted line is at the side, at a distance $1/4W$ from the wall. Picture is reproduced from [18]

We label the flow direction as *forward* ("fwd") and *backward* ("bwd"). If the fluid follows the tips of the grooves, that is called forward flow, the reverse being backward flow.
As we described in section 2.2.1, the tips of the grooves are located in the center of the channel with respect to the y direction. During the experiments some velocity profiles were collected in the center of the channel, and others were collected at the side. The side region is approximately halfway between the center and the wall of the channel (1 mm from the center and 1 mm from the side).
The velocity profiles are collected by recording the motion of tracers along the channel height as described in subsection 2.3.1. The point at the center of the channel is settled as $z = 0$ μm, so that a complete flow profile is collected measuring from $z = -H/2$ to $z = +H/2$. For measures in channels with a smooth wall and a rough one (Smooth-Rough channels) the rough wall is always situated at $z/H = +1/2$.
We checked the position of the ROI in order to have the same position for the measured forward and backward flows. We also decided to move the channel in order to have a gap in the left part of the ROI for every measure session.

Geometry: We distinguish different channels according to their different roughness. The channels used for our measures are summarized in table 2.1. The V-Grooves roughness is identified by the α angle ($\alpha = 30°, 45°, 90°$), and by the grooves' gap g and width w, as previously discussed in subsection 2.2.1 (to clarify is suggested to see the figure 2.4). The height of the roughness was fixed for all the grooves($h = 2.5$ μm). For V-Grooves roughness we also defined $g^* = g/sen(\alpha)$ and $w* = w/sen(\alpha)$, projections on the x axis of g and w.

Emulsion: The emulsion used for the measures, described in section 2.1, was characterized by polydisperse silicone oil droplets. The average droplet diameter was $d = 8.9$ μm and the coefficient of variance ($C.V. = \sqrt{Var(d)}/d \times 100\%$) was $C.V. = 51\%$. The emulsion was diluted at four different volume fractions: $\phi = 0.875,\ 0.80\ 0.75\ 0.60$ (the last one is below the jamming point).

Velocities: We define the plug velocity for the forward direction v_{fwd} as the velocity around $z/H = 0$, estimated averaging the measured velocities in the 3-6 droplets diameters region within the center of the channel. The number of points selected to calculate the mean value depends on the velocity profile considered. In the same way we define the plug velocity for a backward flow v_{bwd}.
To compare v_{fwd} and v_{bwd}, so we define Δv_{plug} as follows:

$$\Delta v_{plug} = \frac{v_{fwd} - v_{bwd}}{v_{fwd}} = 1 - \frac{v_{bwd}}{v_{fwd}} \tag{2.2}$$

§ 2.3.3. Data analysis

The files collected were analysed with a custom routine based on the TrackMate algorithm [55], [56]. The analysis consisted in more steps, presented in this paragraph. In figure 2.8 we summarize all these steps.
The whole procedure can be summarized as follows:

1 **Tracers detection** With a "Difference of Gaussian" (DoG) algorithm, tracers falling in the focal plane of the objective are detected in every frame. Tracers appear as white spots in a dark background. A threshold setting defines the requested difference between tracers and background, and the expected diameter gives to the program the dimension of the objects to search.

2 **Spots selection** The program defines a value called *quality*. It is based on the sharpness of the boundaries of the spot and on the compatibility between the spot diameter and the expected one. In this step we put a filter on the quality value, keeping only the spots that overcome a fixed threshold in order to leave out unreliable spots.

3 **Tracking** At this point, the program compares the position of spots taken in different frames. To properly reconstruct tracers tracks it is necessary to set the following parameters.

- *Linking max distance*, the maximum distance allowed between two spots in the same track
- *Gap-Closing max distance*, the maximum distance allowed to link two different segments of a track. It is useful if a tracer is not recorded in one frame, because the track could be obtained anyway.
- *Max Frame Gap*, the maximal frame interval admitted between two spots of non-consecutive frames. It is related to the detection of gap-closing events.

4 **Track filtering** We finally apply filters directly on tracks to retain only reliable tracks:

- *Track mean quality*, calculated averaging the values of the quality of the points in the same track.
- *Number of spots*, obtained just counting the number of spots in the track

5 **Speed analysis** Once recorded the tracks, it is easy to calculate the mean velocity related to each one of them. The exposure time defines the time interval Δt between a frame and the following one. The calculated distance Δx is the one between consecutive spots in a track. The average velocity between two points is calculated as $v = \Delta x/\Delta t$ and then the mean velocity is obtained by averaging these values.
At this point the velocity of a z is obtained averaging mean velocities for all tracks.

6 **Flow profiles analysis** Repeating the previous steps for every z, it is possible to obtain the velocity related to each plane. In this way we reconstruct the complete flow profile inside the channel.

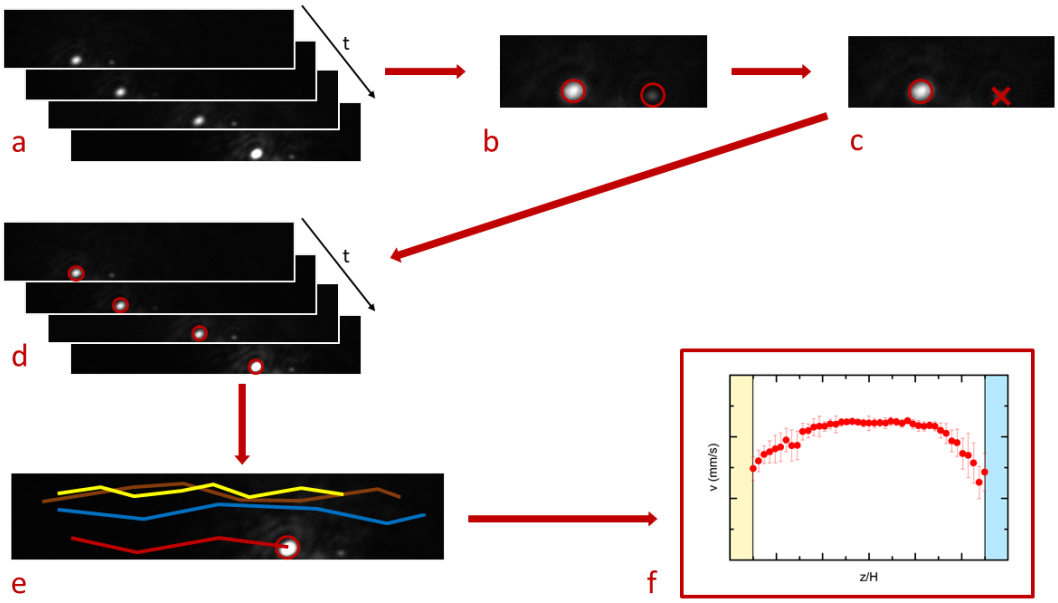

Figure 2.8 : Scheme representing the steps in data analysis. We start from the image stack (a) and we analyse every frame with a DoG algorithm (b). We apply filters on spots (c) and we repeat this procedure for every frame, obtaining a series of spots for the image stack (d). The tracks are obtained from the spots(e) and a filter is applied. Finally, the velocity is obtained by averaging. Repeating his for every z we obtain the Velocity profile (f).

Chapter 3

Results

In this Chapter we describe experimental results, showing the behaviour of a concentrated emulsion flowing in microfluidic channels.
In particular, we focus on the effects obtained by introducing the herringbone roughness (or V-Grooves roughness).
The chapter is organized as follows. In section 3.1 we analyse the flow of a Newtonian viscous fluid in a herringbone patterned microfluidic channel. Then, in section 3.2 we discuss the flow of concentrated emulsion as a function of the flow direction showing the effects given by the V-shaped roughness, and emphasizing the difference with the Newtonian behaviour observed in 3.1.
In section 3.3 we discuss the effect of the centrifugation on the emulsion stored in syringes, explaining the reasons why this may influence our measures. Then we describe the experimental procedures followed to avoid these problems.
Finally, we describe the effects obtained by changing parameters like the angle of the V-Grooves (section 3.4), the applied pressure drop Δp (section 3.5) and the gap of the grooves (section 3.6).
Finally in section 3.7 we discuss the results, giving some explanations for the observed effects.

§ 3.1. Newtonian viscous fluids in herringbones decorated channels

First, we measured the velocity profile of a Newtonian fluid in a herringbone decorated channel to assess the role induced by this geometry. The fluid was pure anhydrous glycerine (Sigma-Aldrich) flowing in channels characterized by $w = 8\ \mu$m, $g = 8\ \mu$m and $\alpha = 45°$.
In figure 3.1 we can report different velocity profiles for glycerine at two different pressure drops: $\Delta p = 0.1, 0.3\ bar$. For every pressure drop we collected one velocity profile for the forward flow and one for the backward. Empty dots stand for measures collected at 0.3 *bar* and filled dots depict measures at 0.1 *bar*. Upside triangles depict forward measures and downside triangles depict backward measures. Every profile was recorded in the channel center ($y = 0$) as described in 2.3.2.

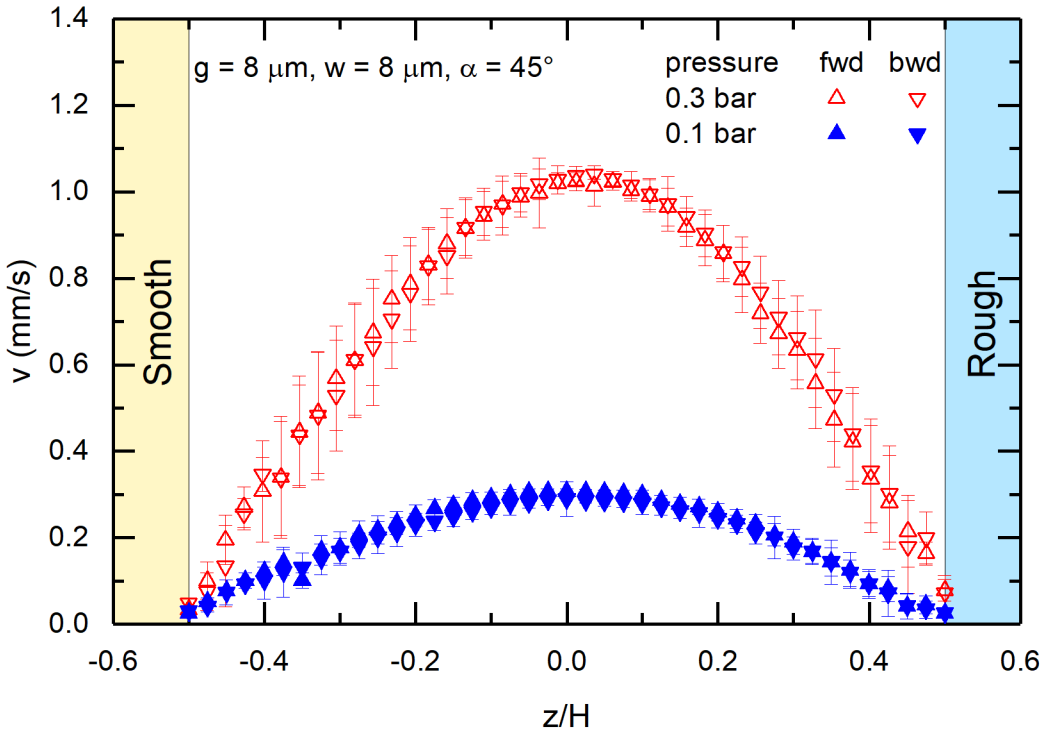

Figure 3.1 : Velocity profiles $v_{flow}(z)$ measured for glycerine flowing in a microfluidic channel patterned with V-Groove roughness.

For both pressure drops, forward and backward profiles are overlying, if we consider the error bars. This fact means that the asymmetric roughness has no effect on a Newtonian fluid as the glycerine. Moreover, we can see that every flow profile shows a parabolic shape, this feature being is typical of Poiseuille flows for low Reynold numbers ($Re \sim 10^{-5}$). We also see that the slip velocity at the walls is 0 for every profile, this is a characteristic of Newtonian, viscous fluids that does not persist for our emulsion.
Conversely, flow profiles are slightly asymmetric with respect to $z/H = 0$. The effect of the roughness could result in this asymmetry but it is too small to be quantified and anyway it is out of the scopes of this work.

§ 3.2. Center versus Side

In figure 3.2 we can report the velocity profiles for an emulsion at $\phi = 0.875$ flowing through a herringbone decorated channel. The channel is the same used with glycerine, ass described in section 3.1 (V-Groove roughness with $w = 8$ μm, $g = 8$ μm and $\alpha = 45°$). The pressure drop was $\Delta p = 3$ bar.
We collected a forward profile and a backward profile at the center of the channel. These profiles are represented by filled dots (upside and downside triangles respectively).
We also collected a forward profile and a backward profile shifted of ~ 1 mm along the cross section, with respect to the center of the channel. This is reported with empty dots. A scheme for these measures is presented in subsection 2.3.2. Again, the upside triangle stands for the flow in forward direction and the downside triangle indicates the backward direction. The rough wall is at $z/H = 0.5$ while the smooth wall is at $z/H = 0.5$.

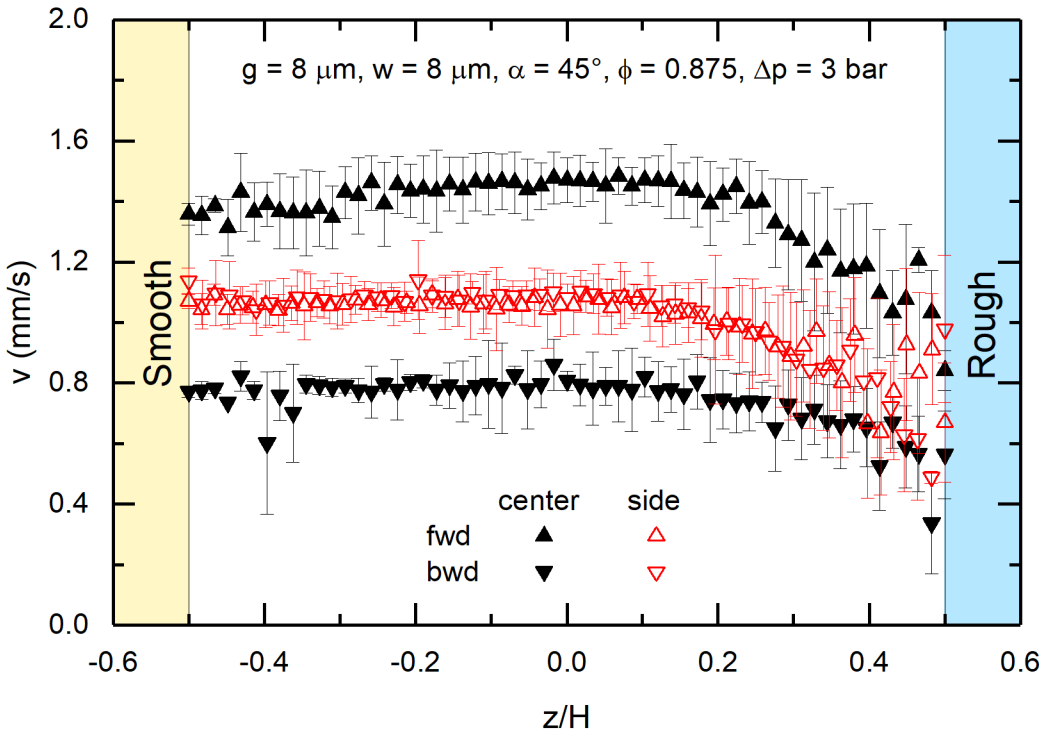

Figure 3.2 : Velocity profiles $v_{flow}(z)$ measured for an emulsion flowing in a microfluidic channel patterned with V-Groove roughness. v_{flow} is represented in function of z/H.

First of all we can see that the forward and backward profiles collected in the channel center are different. This fact suggests that the asymmetric roughness of the channel has different effects on the flow for different directions.
Moreover, forward and backward profiles collected on the side are overlapping, meaning that, in this region, the flow keeps the same behaviour in both directions. We deduce that the asymmetric roughness introduce a difference in the plug velocities only in the middle of the channels' cross section, while the difference is vanishing on the sides. For this reason, we focused on the enhancement of the

plug velocity induced at the center of the channels' cross section.
In particular, the forward profile measured at the center is faster than the others. In parallel, the backward profile is slower than all the others when the emulsion is flowing at the side of the channels' cross section. For these reasons the effect of the roughness is marked in the channel center, and it

- helps the flow on the direction suggested by the tips of the grooves
- hinder the flow on the backward direction

Moreover, we can observe that every profile is asymmetrical with respect to $z/H = 0$. In fact each profile shows a difference in the slip velocities between the smooth and the rough surface due to the presence of the roughness, as described by [12, 13]. The profile shows a disordered behaviour near to the rough wall ($z/H \gtrsim 0.2$). This is consistent with the occurrence of plastic rearrangements induced by the roughness as reported in [12, 13]. Due to these large fluctuations it is not easy to estimate the slip velocities for these velocity profiles, and we just underline the difference of wall slip trend between the smooth and the rough walls.
It is noteworthy to notice that the plug region, where the fluid is flowing as a solid-like disordered structure, occupied roughly the half of the channel ($z/H \in [-0.2; 0.2]$). Since we are working above the jamming point of the emulsions, this implies that the corresponding yield stress results higher even of the stress close to the walls (i.e. the shear regions of the emulsion flow).
The effect of the smooth wall would have been more pronounced with a more-liquid behaviour. To help the fluidization it is possible to increase the pressure or to dilute the emulsion. Unfortunately, 3 $bars$ was the experimental limit imposed by our apparatus (higher pressures may damage the channel sealing). For this reason the emulsion was diluted at a lower volume fraction in the other measures.
If we focus on the region near to the rough wall ($z/H \in [0.2; 0.5]$), we can see that the velocity profile is disordered, but the velocity globally decreases near to the wall.

§ 3.3. Volume fraction gradients

We are interested to understand how $\Delta v_p lug$ (introduced in section 2.3.2) changes with respect to different parameters (α, Δp, g). A quantity that may affect Δv_{plug} is also the volume fraction. This dependence will be discussed in detail in section 3.7. In this section we aim to discuss the dependence of Δv_{plug} when the volume fractions of flowing emulsions is not uniform. In fact, while the volume fraction of a syringe is known by preparation, it is not possible to determine the effective volume fraction of the emulsion as it flows in the channel. In other words, we know exactly the quantity of silicone oil and dispersed phase in every emulsion syringe, but there are uncontrollable local fluctuations.
In particular, the centrifugation is a process essential to remove the air bubbles trapped in the emulsion, as we explained in 2.1, and it is the only reliable method reported in literature. However, as a drawback, this method may change the local volume fraction of the emulsion along the centrifuged syringe.
This is due to the density mismatch of the emulsion constituents. In fact the dispersed phase density is $\rho_{oil} = 0,97$ g/ml, while the density of the continuous phase is $\rho_{c.p.} = 1,14$ g/ml. As a consequence, under centrifugation the continuous phase is pushed on the bottom of the syringe while the dispersed phase migrates on the top (see figure 3.3).

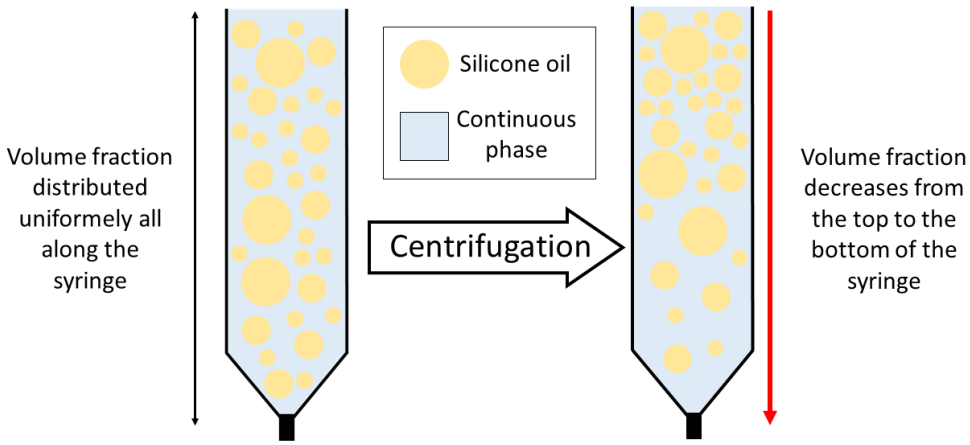

Figure 3.3 : Scheme representing the effect of centrifugation on an emulsion syringe.

The resulting volume fraction is slightly increasing from the bottom to the top of the centrifuge vials. We point out that this gradient of droplets concentrations along the syringe (vial) dosing the emulsions is pretty small. For example, after centrifugation, rheological measurements hardly detect tiny differences of the yield stress from bottom to top of the vial. To address the importance of tiny gradients of the volume fraction, we performed time resolved measures of the forward and backward flows in a channel with two smooth walls (smooth-smooth channel). The only difference between these flows is given by the direction, but the channel is symmetrical, so the velocity profile for the forward flow and the one for the backward flow should be the same. In figure 3.4 we can see different flow

profiles of a concentrated emulsion ($\phi = 0.80$) in the smooth-smooth channel with a stable pressure drop $\Delta p = 1.5$ bar. Upside triangles represents forward flows while downside triangles depict the velocities for backward flows. The chronological order of these measures is given by the number in brackets in the legend:(1) stays for first forward flow, (2) first backward flow, (3) second forward flow, (4) second backward flow. The sequence reflects the measuring procedure: a couple of forward and backward flows was collected in the beginning and after that we collected a second couple of forward and backward flows. The color indicates a complete dataset (forward/backward).

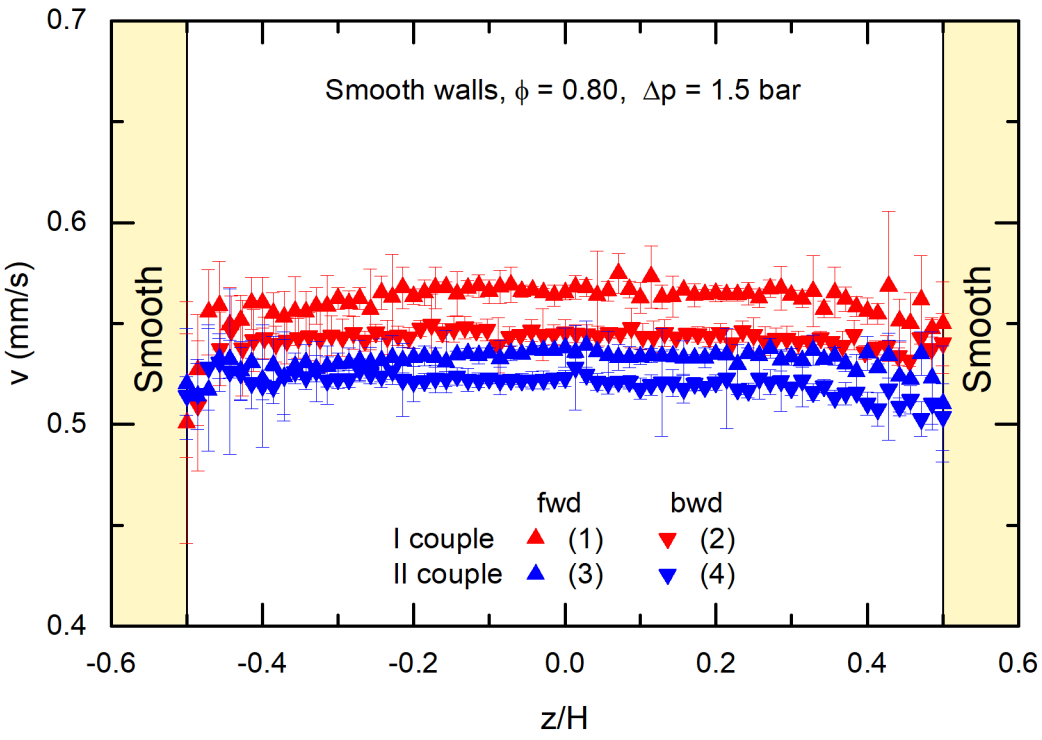

Figure 3.4 : Velocity profiles $v_{flow}(z)$ measured for emulsion flowing in a microfluidic channel with smooth walls. The number in brackets near to the dot in legends stands represent the chronological label of the measure.

The graph shows an interesting behaviour: every velocity profile is different from the others. In particular, we see that $v_{fwd}(1)$ for the first forward profile is faster than $v_{bwd}(2)$ for the first backward profile. So we obtain a $\Delta v_{plug} \neq 0$, that would be an unexpected result for a completely symmetric channel. Moreover the v_{fwd} for the second couple of measures (green upward triangles) is still slower than the velocities for the previous measure, and so does the last measure of v_{bwd}. So, we observe that the velocity of the emulsion is continuously decreasing, suggesting that the effect is not given by a defect in the channel, since it is not related with the direction.

To better investigate this effect we decided to perform time resolved measures of v_{plug} only. We settled a pressure drop ($\Delta p = 2$ bar) and we let the emulsion flow, measuring tracers in a fixed point of the channel ($z/H \sim 0,\ y \sim 0$). We collected 1000 frames at 1000 fps once every 100 s. For this measure we used two emulsions with a different volume fraction ($\phi = 0.80,\ 0.75$). In this way we are sure that the effect is not related to a specific syringe or volume fraction.

Results are shown in figure 3.5(a),(b), reporting the normalized measured velocity as a function of the time $v_n(t)$. The velocity was normalized by the first value taken at the time $t_0 = 100$ s ($v_n(t) = v(t)/v(t_0)$), so that $v_n(t_0) = 1$.in figure 1.2

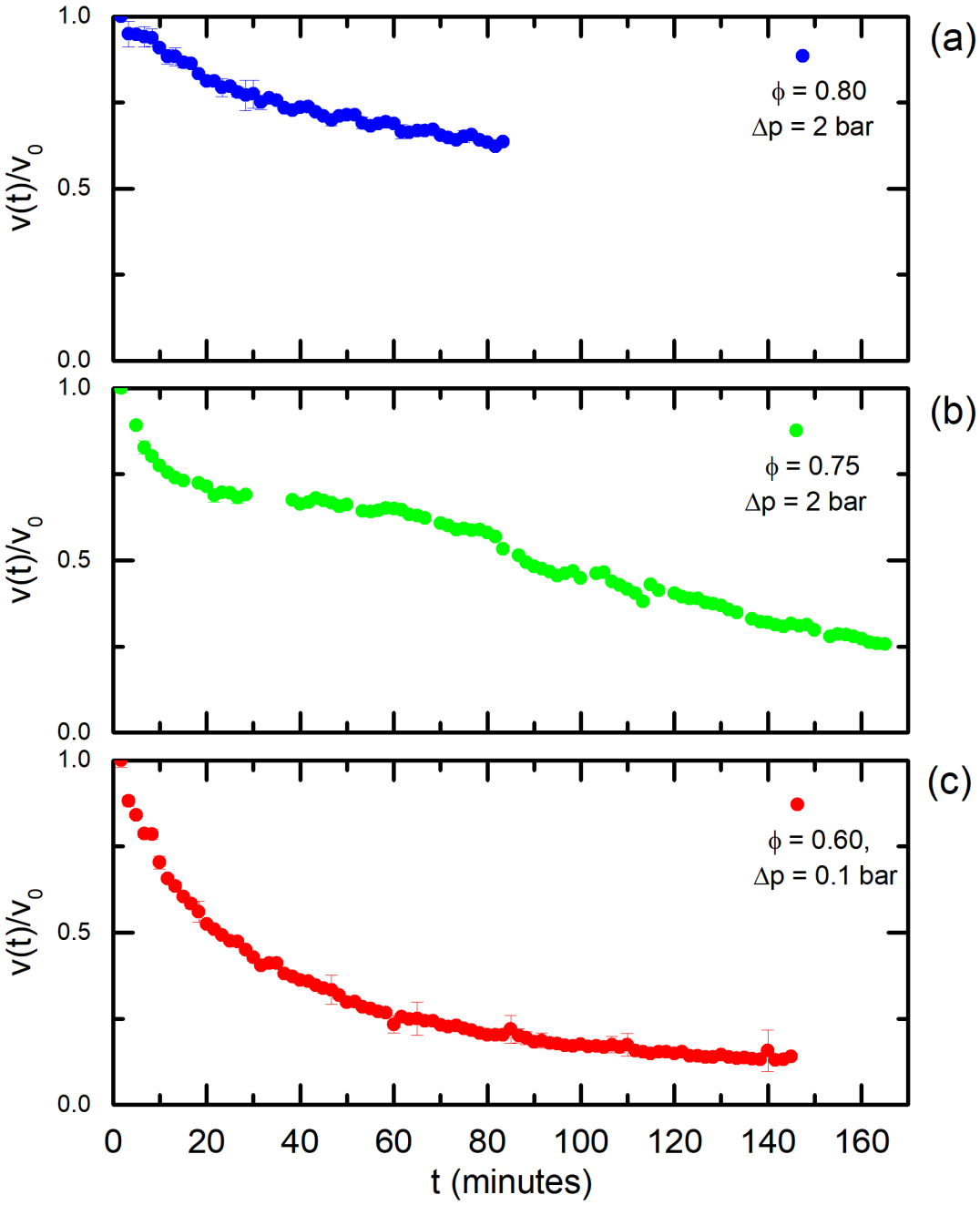

Figure 3.5 : Normalized velocity $v(t)/v_0$ in function of the time t for centrifuged emulsions with different volume fractions flowing in the same smooth-smooth channel. Figure (a) refers to $\phi = 0.80$, figure (b) refers to $\phi = 0.75$ and figure (c) refers to $\phi = 0.60$ (below the jamming point).

This measures give a glaring result: the plug velocity strongly depends on the quantity of emulsion fluxed from the syringe.

To complete this description, we performed time resolved measures also of emulsions below the jamming point ($\phi = 0.6$). We collected three flow profiles with this emulsion, flowing ~ 1 ml between

every measure and the following. This emulsion is very fluidized so the pressure drop necessary to make it flow is very low. For these measures we settled $\Delta p = 0.1$ bar. Results are reported in figure 3.6. From this figure we can see that the collected measures lead to overlapping profiles, so

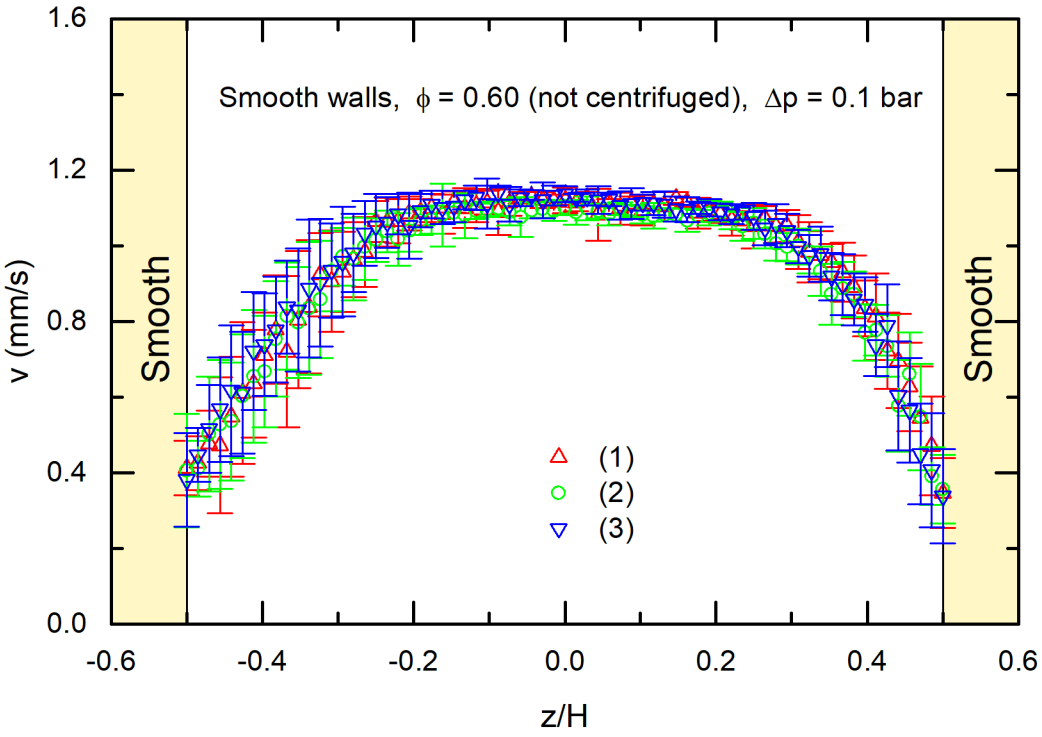

Figure 3.6 : Velocity profiles $v(z/H)$ in function of z/H for a not centrifuged emulsion in a smooth-smooth channel.

we conclude that we could not see the volume fraction effect for a not centrifuged emulsion. To be sure that the centrifugation is the cause of the behaviour observed in the previous measures, we centrifuged also the $\phi = 0.60$ emulsion to see if the effect would be observed also in this case. For this measures we adopted $\Delta p = 0.1$ bar. We collected 1000 frames at 1000 fps once every 200 s in the channel center, reporting the results for v_n in figure 3.5(c). We can see that the velocity is slowing down also in this case, and we have the evidence that this effect is due to the centrifugation procedure.

Procedure to avoid the volume fraction effect The observed behaviour caused by the centrifugation of the emulsion could have been a problem for our measures. A procedure to avoid this effect was necessary, otherwise it would be impossible to compare results from different channels.
We need to compare measures in different channels using emulsion with the same volume fraction for every measure. For this reason we decided to store the diluted emulsion in three syringes. Inside every syringe we stored the same amount of emulsion, and then we centrifuged all the syringes at the same time. In this way we can be sure that the centrifugation has the same effect on the emulsion for every syringe.
At this point we compare the emulsion flow in the smooth-smooth channel as reported in figure 3.7.

Every color represents the flow of emulsion from a different syringe. Every measure was done with $\Delta p = 1$ bar As we can see the velocity profiles are overlapping, so the procedure is good. Some

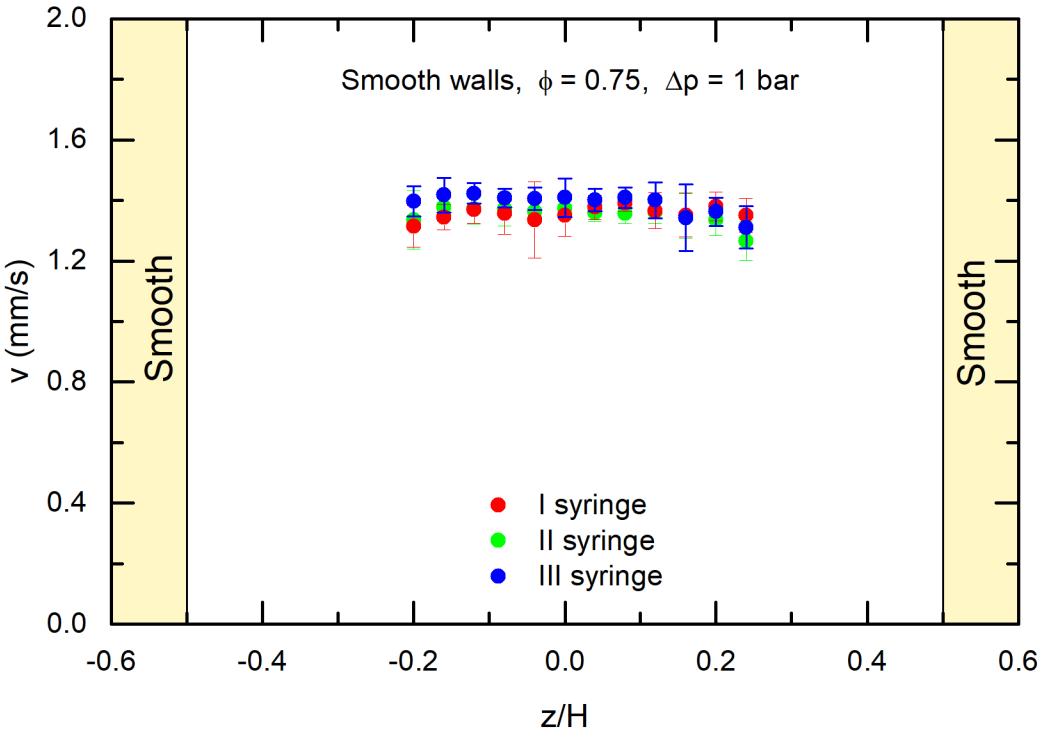

Figure 3.7 : Flow profiles for a $\phi = 0.75$ emulsion from three different syringes. The three syringes were centrifuged together and the same amount of emulsion was fluxed from every syringe before taking this measure.

fluctuations are still observed, but we can estimate that the total difference is $\sim 4\%$. This difference is given also by other problems as fabrication defects, pressure control and temperature.

When we want to compare the emulsion flow in different channels, we take a different syringe for each channel. Before doing the measures, we check the amount of emulsion removed from every syringe, and we perform a test in a smooth-smooth channel. With this procedure we can get the same volume fraction for each set of measures.

Verifying the effect of the roughness Once observed the emulsion effect, we need to be sure that the difference between forward and backward flows in channel with V-Groove roughness is effectively given by the roughness and not by the volume fraction. For this reason we decided to do the following test. We measured four times the flow in the center of a channel with V-Grooves ($g^* = w^* = 21$ μm, $\Delta p = 1.5$ bar). We alternated a forward flow to a backward flow, and the chronological order of the measures is written in brackets. Results are reported in figure 3.8. Also in this case upside triangles represents forward measures while downside triangles represent backward measures. Red dots represents the measures for the first "forward-backward" couple, while green dots represent the second couple.

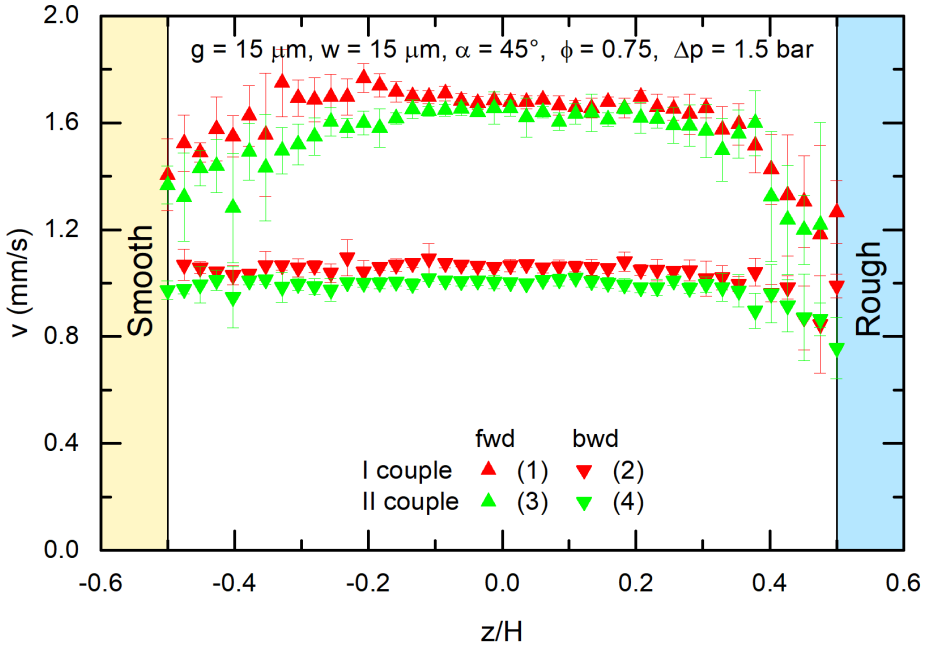

Figure 3.8 : Velocity profiles representing $v(z)$ measured in the center of a channel characterized by V-Grooves. The chronological order of the measures is written in brackets.

We can see that the difference between forward and backward profiles (the effect that we want to study) is greater than the difference between different measures taken with the same flow direction. We can conclude that there is an effect given by the volume fraction, but it is less marked than the effect given by the groove roughness.

Final remarks In this section we studied the effects on the flow induced by the centrifugation process. We have seen that it results in a volume fraction gradient along the emulsion syringe. This should be a problem when we want to compare different measures but we presented our solution: storing the same quantity of the same emulsion in more syringes and centrifuging all the syringes together. When we need to compare more measures, we use a different syringe, checking that the amount of emulsion removed is the same. This method does not delete the volume fraction gradient, but we are sure that the compared measures are all affected by the same effect. Comparing a series of measures we also saw that the effect of the V-Groove roughness is more pronounced than the effect given by the changing in volume fraction.

§ 3.4. Effect of the angle of the V-Grooves roughness

In this section we want to describe how the angle of the V-Grooves roughness affects the emulsion flow.
If we want to see the effect of the angle, we need to be sure that the angle is the only parameter to be changed. For this reason our measures are collected at a fixed pressure drop ($\Delta p = 1\ bar$), with the same volume fraction for all the measures ($\phi = 0.75$), using the procedure described in section 3.3. For these measures we used channels with a fixed projection on the flow direction of gap g and width w (respectively g^* and w^*). By fixing g^* and w^*, every droplet undergoes the same number of obstacles in the same length, so we can really compare the angle effect (fixing g and w this comparison would not be possible). For this reason we fixed $g^* = 15\ \mu$m and $w^* = 15\ \mu$m.
We used microfluidic channels with V-Grooves with $\alpha = 30°,\ 45°$, and with straight grooves (considered as $\alpha = 90°$ V-Grooves). In figure 3.9(a) we show different velocity profiles collected at the different angles. Upside triangles depicts forward flows while downside triangles depicts backward flows. Data for $\alpha = 90°$ are presented with filled blue dots, $\alpha = 45°$ are presented with empty green dots and $\alpha = 30°$ are presented with red transparent dots.

As we can see from the picture, the plug velocity assumes very different values for the different sets of data. In particular we see that velocity of the forward profile increases if the angle decreases. On the contrary the velocity of the backward profile decreases with the decreasing of the angle. This combined effect leads to an increasing difference between v_{fwd} and v_{bwd} as the angle decreases.
For $\alpha = 90°$ we can consider the two profiles as overlapping, in fact the slight difference between them could be given by the effect described in section 3.3 or by other causes like fabrication defects. Anyway $\Delta v_{plug}(90°) \sim 7\%$ To see this effect we estimated the values of Δv_{plug} (as defined in equation 2.2) for every α. In figure 3.9(b) we can see, as expected, that Δv_{plug} assumes the greater value for the smallest angle, it decreases for $\alpha = 45°$ and it goes to 0 for the straight Grooves. The emulsion behaviour is explained in section 3.7.

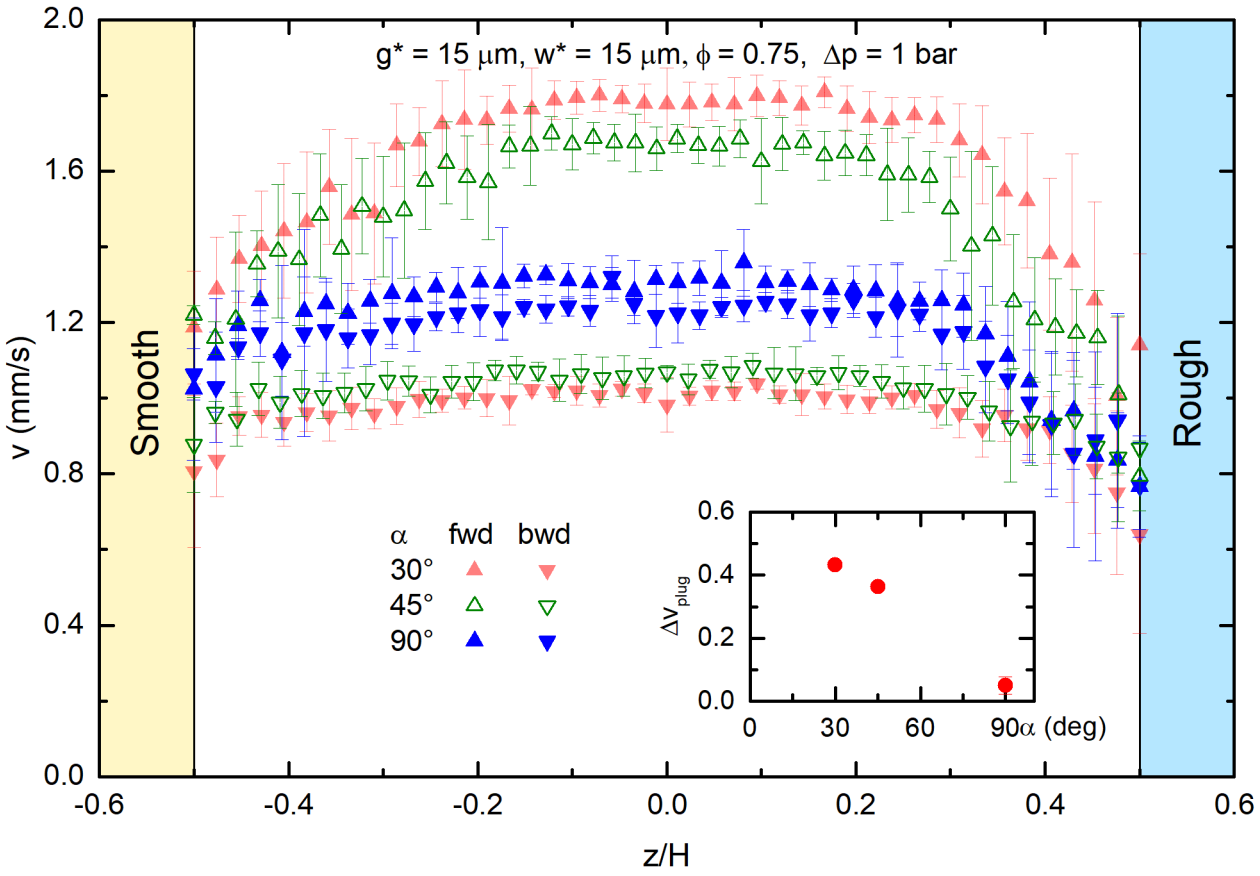

Figure 3.9 : Pictures representing the angle effect in different channels (Smooth-Rough channels characterized by V-Grooves roughness with $\alpha = 30°,\ 45°,\ 90°$). In figure we can see forward and backward flow profiles for these channels. In subfigure we can see the calculated Δv_{plug} in function of α. (remember that $\Delta v_{plug} = (v_{fwd} - v_{bwd})/v_{fwd}$)

§ 3.5. Effect of the pressure

In this section we study the effect of the pressure on the flow of the $\phi = 0.75$ emulsion in herringbone decorated channels. In particular we compare forward and backward flows measured in the channel center at different settled pressures.

We focus on the effect on v_{plug}, neglecting the effect on the walls of the channel.

In figure 3.10(a) we can see v_{fwd} and v_{bwd} for a Smooth-Rough channel with the V-Groove roughness ($\alpha = 30°$ and $g = w = 4\ \mu$m). Velocities for forward flows are represented with red upside triangles while velocities for backward profiles are depicted with blue downside triangles.

Obviously we can see that v_{fwd} and v_{bwd} increase with the pressure, but we also see that v_{fwd} is always faster than v_{bwd}, except for 0.2 *bar* where the emulsion is barely flowing, and the two velocities are nearly the same.

As we increase the pressure, the difference between v_{fwd} and v_{bwd} increases. To study this effect we calculate Δv_{plug}, as we show in figure 3.10(b). We see that Δv_{plug} increases with the pressure, but the rise seems to slow down with high pressure. Unfortunately, measures at higher pressures were

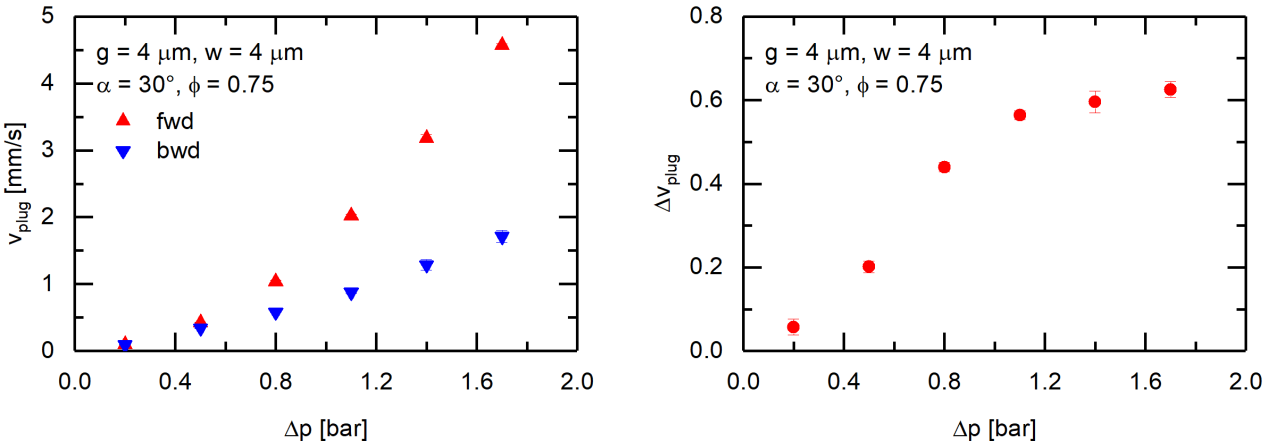

(a) v_{fwd} and v_{bwd} vs

(b) Δv_{plug} versus Δp

Figure 3.10 : Effect of the pressure on the emulsion flow. In figure (a) are presented v_{fwd} and v_{bwd} for different Δp. Figure (b) shows the values of Δv_{plug} (eq. 2.2) in function of the pressure drop.

not allowed by the experimental apparatus (as we can see at 1.7 *bar* the emulsion is flowing with $v_{fwd} \sim 5$ mm/s, the fast camera could not support a faster flow).

§ 3.6. Effect of the gap of the V-Grooves roughness

In this section we wanted to describe how the gap of the V-Grooves influences the flow of the emulsion. We decided to use the channels with the smallest and the biggest gap projection on the x axis:

- Channel 1 (narrow gap): $g = 4\ \mu\text{m},\ w = 4\ \mu\text{m}, \alpha = 30°$ $(g* = w* = 8\ \mu\text{m})$
- Channel 2 (wide gap): $g = 12.5\ \mu\text{m},\ w = 12.5\ \mu\text{m}, \alpha = 30°$ $(g* = w* = 25\ \mu\text{m})$

These channels were created referring to the article [13]. They saw the effects of the straight roughness on a concentrated emulsion in function of the gap, underlining two different scenarios: one for wide gaps ($g > 3$ droplet diameters) and one for narrow gaps($g < 2$ droplet diameters). For the microfluidic channels studied in this thesis, V-Groove roughness was built relying on the cited article, and the gap was adapted to that dimensions. Unfortunately the mean diameter of a droplet in our emulsion ($\sim 9\ \mu\text{m}$) is bigger than the expected (for [13] $d = 4.7\ \mu\text{m}$). For this reason, the bigger gap built for our experiment is ~ 3 droplet diameters, and we were not sure to see the two scenarios.
Figure 3.11 shows different values for Δv_{plug}. Red dots refers to the flow in the channel with the narrow gap roughness, while blue dots depict measures in channels with a wide gap.

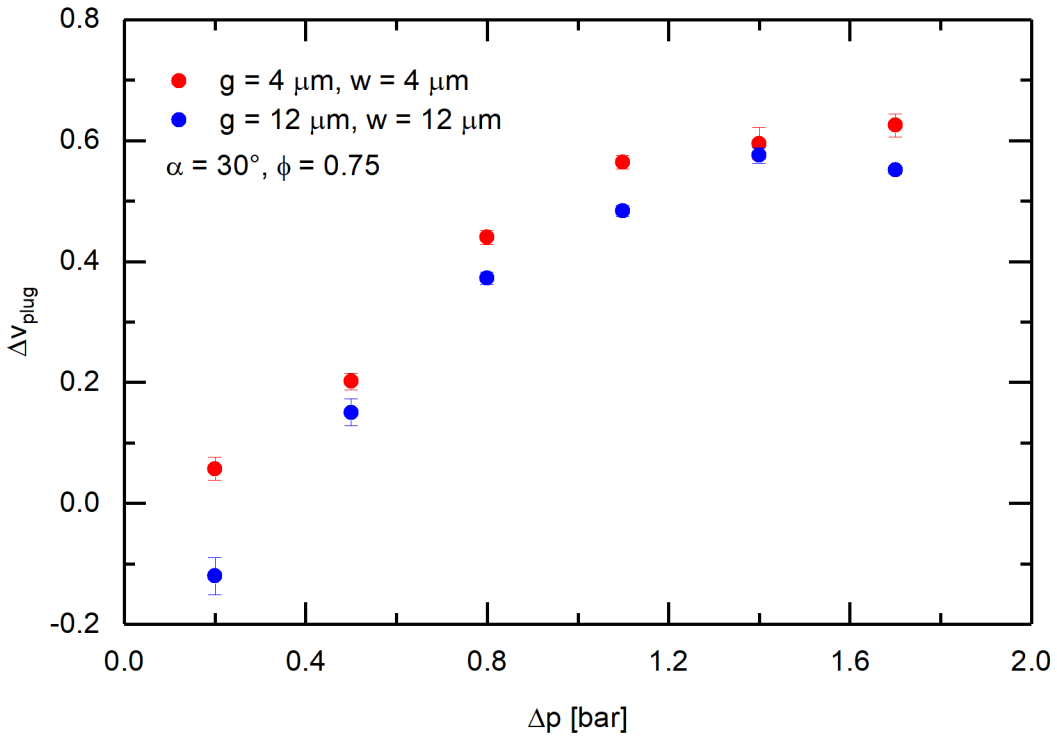

Figure 3.11 : Comparison between the flow of concentrated emulsion in two microfluidic channels with different gaps. The picture shows calculated Δv_{plug} in function of the pressure.

We can see that the curves are very similar, so we are in the same scenario for both gaps. For the wide gap, Δv_{plug} assumes a negative value at 0.2 *bar*, at this pressure the emulsion flows slowly, and

the rate of rearrangements is practically null. This negative value could be explained as a fluctuation of the system that is more visible since the droplets are moving slowly. We can conclude that in the experiment conditions, we could not see any marked effect given by the changing of the gap.

§ 3.7. Discussion

In this section we propose a simple description to explain the effects observed in figures 3.1, 3.2, 3.9 and 3.10 and the differences between the flow profiles presented. In particular we explain

- why forward and backward profiles are different for a concentrated emulsion in the channel center
- why this difference does not affect the flow of the emulsion at the channel side
- why this difference between profiles is not observed for a Newtonian fluid.
- how the angle affects the flow
- why the pressure enhance Δv_{plug} and why the enhancement stops at bigger pressures.

All these differences on the flow are generated by a different micro-mechanical behaviour of the emulsion.

Center versus Side First of all we consider the emulsion droplets flowing in the the same direction of the V-Grooves tips as presented in figure 3.12(a).

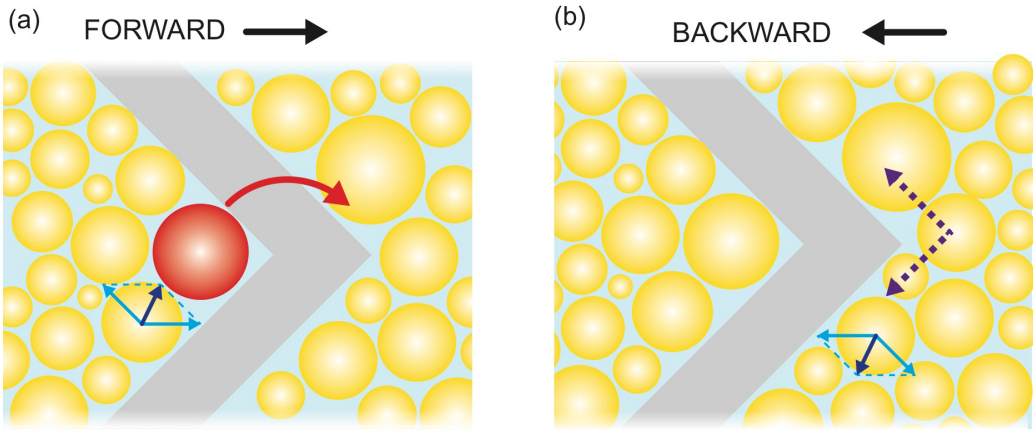

Figure 3.12 : Scheme representing the flow of a concentrated emulsion across the roughness of a herringbone decorated channel. In figure (a) oil droplets are flowing in the center of the channel in forward direction. In figure (b) they are flowing in backward direction. Pictures taken from [18]

This configuration refers to a flow along the x axis in the forward direction. The applied pressure drop Δp generate the flow of the droplets in the channel. If a droplet falls into the gaps provided by the roughness, it can slide along the groove, pushed by other droplets, instead of jumping across it. In figure 3.12 we show the two forces acting on the droplets. One is given by the pressure drop, and it has the same direction and verse of the flow. The other is given by the normal force of the roughness, and it is perpendicular to the groove. Summing these forces, we obtain the resulting force represented

by blue arrows, as we can see it is parallel to the walls of the grooves.
This results on a non-stop pushing to the center of the channel for all the droplets. When a droplet reaches the center, it jumps across the grooves, pushed by the other droplets from the sides and from the back. Obviously, if a droplet finds other droplets in the center, it could both jump across the groove or push them until they jump, so the dynamics gets more complicated.
If a droplet overcomes the obstacles, the jump could activate a plastic rearrangement, hence we conclude that, for an emulsion flowing on the forward direction, rearrangements on the center occur with a higher rate than rearrangements on the side.
A higher rate of plastic rearrangements affects the flow by increasing the fluidity, and finally a higher fluidity affects the velocity profile inducing a greater v_{plug} and a more pronounced Δv_{slip}
Comparing with straight grooves we can see that the overcome of obstacles is now emphasized by the droplets motion from the side to the center.

Let's consider the backward direction, as represented in figure 3.12(b). In this case the geometry leads droplets to the sides. In fact the droplet is not confined, and the resultant force guides the droplet to sliding along the wall. This effect prevent the storing of droplets in the center and avoids the rearrangements.
If the droplets rearrange less frequently, the fluidization's rate is smaller, and that results in lower values for v_{plug} and for Δv_{slip}. Now we focus on the side of the channel, represented in figure 3.13.

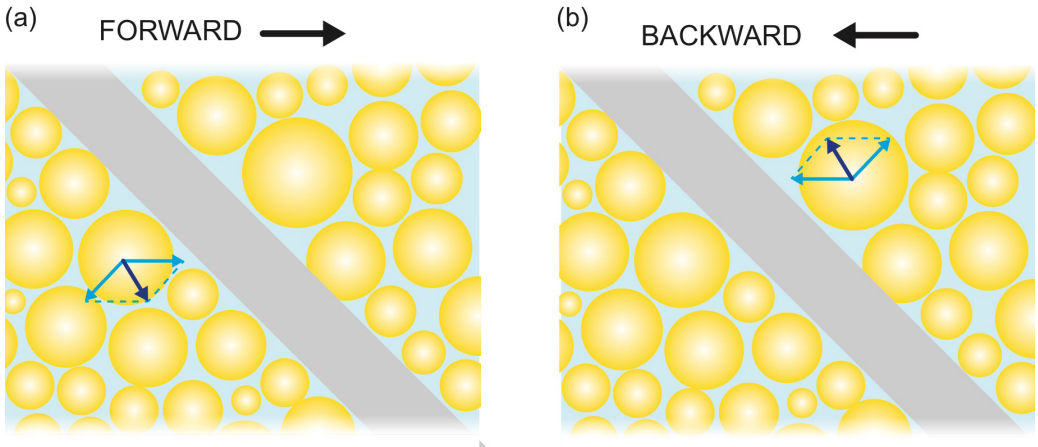

Figure 3.13 : Scheme representing the flow of a concentrated emulsion near to the roughness of a herringbone decorated channel. In figure (a) oil droplets are flowing at the side of the channel in forward direction. In figure (b) they are flowing in backward direction. Pictures taken from [18]

It is easy to see that in the situation described in the central region, the geometry was different for backward and forward directions, while on the lateral region the difference is less pronounced. Far enough from the center and from the lateral walls, droplets see the roughness as a tilted groove. In both directions the droplet is guided by the same geometry, for this reason it flows in the same way in forward and backward direction.
Every time a droplet falls into the a groove, it slides along the wall and sometimes it jumps across the groove. Every time a droplet overcome the obstacle, it provides a plastic rearrangement. If there are no differences between forward and backward geometry, the rearrangements rate remains the same in

both directions.
The same rate of rearrangements leads to the same fluidization, and this explains the same v_{plug} and the same profile in both the directions. Now that we explained the general behaviour observed for section 3.2, we can consider the other effects.

Newtonian fluid Now, if we consider a Newtonian fluid as in section 3.1, we see that forward and backward profiles are overlying. In this case the asymmetric roughness does not influence the velocity profiles. In fact, glycerine molecules are too small to interact with the roughness, and there are no plastic rearrangements. This does not provide differences between forward and backward velocity profiles, as seen in Figure 3.1 for every pressure.

Effect of the angle Now we consider the section 3.4. In Figure 3.9 we saw that Δv_{plug} was enhanced by the decreasing of the angle.
If the $\alpha = 90°$ there are no differences between the geometries seen from droplets in forward and backward direction. For $\alpha = 30°, 45°$ there is no symmetry between forward and backward. By changing the angle, we obtain a different normal reaction to the droplet flow. Different angles lead to different effect, according to the normal reaction given by the wall of the grooves. If we consider a great α, the direction of the normal reaction of the wall is mostly on the flow direction and the deviating component acting on the droplet is weak. If α is small, the component of the normal reaction that points to the center of the channel is bigger, and the droplet is guided to the center. Hence we obtain a guiding effect more pronounced with smaller angles.
If the flow is moving on the forward direction, the pronounced guiding effect (as the one for smaller angles), enhances the stress, and then the rate of plastic rearrangements. As explained before, a greater rate of rearrangements leads to a greater fluidization and to a faster flow.
For the backward flow the outcome is the opposite. The greater guiding-effect provided by smaller angles deflects droplets from the center. Therefore plastic rearrangements in the center are avoided and the stress is lightened. Finally, for a backward profile, the fluidization decreases with the decreasing of the angle.

Effect of the pressure The main effect observed in section 3.5 was the enhancement of Δv_{plug} given by the increasing of Δp. This effect is explained as follows.
At lower pressures the applied force is not enough to overcome the yield stress, so there is no fluidization. As we increase the pressure, the force acting on every droplet increases, and so does the stress that generates rearrangements. If the pressure increases, the fluidity of the system is enhanced by the increasing rate of rearrangements and the emulsion flows faster.
Very high pressures can continuously generate rearrangements, and the emulsion gets so fluidized that the enhancement provided by the smooth wall starts to be secondary.

Conclusions

This thesis studied the emulsion flow in microfluidic channels, characterizing the effects of the wall roughness on the flow. The roughness affects the flow by enhancing the fluidization. This effect is caused by the stress accumulated in elastic deformations, released through plastic rearrangements. From [12, 13] we know that the surface roughness triggers rearrangements and enhance the fluidization. In this thesis we studied in deep these effects, investigating the effect of the asymmetrical shaped grooves. The study of these effects shape is completely new and the observed results are reported below.
We could observe different flows for different geometries, and for different flow conditions. Our results could be used to control the flow of soft-glassy materials in microfluidic channels, by adjusting the surface roughness.

(i) Effect on non-Newtonian fluids Comparing the flow of Glycerol with the dense emulsion flow, we observed that the roughness affects only the non-Newtonian fluid. This is an interesting result because the different behaviour could lead to a device that affect only one kind of fluid.

(ii) Effect of the asymmetric roughness The forward flow compared with the backward enlightened a different behaviour for different flow directions. We have seen that the V-Groove roughness enhances the forward flow in the channel center, and that the backward flow in the center is even slower than the flow at the side. Moreover we observed that the flows at the side have overlapping velocity profiles.
We concluded that the effect of the fluidization is observed only in the channel center, and we gave an explanation for this behaviour.

(iii) Effect of the angle Comparing forward and backward flows for dense emulsions in the channel center, and we tuned the V-Grooves angles. We observed that the enhancement for the forward flow increases with the decreasing of the angle. This was explained with the accumulation of a greater stress at the channel center in the forward configuration, that leads to a greater fluidization of the emulsion. On the other hand the enhancement given by the roughness in the backward flow is less marked for smaller angles. The V-Grooves relieve the stress from the center, so the rearrangement rate decreases and the fluidization goues down with it.
This effect was never studied before, and the control of the roughness allows us to obtain a marked difference between flow profiles in the two directions, or to reduce or annihilate this difference.

(iv) Effect of the pressure We observed that the difference between forward and backward flows is low at low pressures, and it increases with the increasing of the pressure. The enhhancement for the forward profile seems to stop at the higher pressures, but the limits of our experimental apparatus did not allow us to investigate this behaviour. Anyway it is interesting to observe that the difference between flows could be enhanced and controlled by an increase on pressure.

(v) Effect of the gap We conclude saying that in our conditions we did not observe considerable effects given by the changing of the gap. In other works were observed effects from the changing of this parameter. In [13] they show that the changing of the gap leads to two different scenarios in relation with the size of the droplets and of the gaps. Comparing our conditions with their, we concluded that in our case the relation between droplet size and gaps was linked to only one of the two scenarios.

Bibliography

[1] A. J. Liu and S. R. Nagel, "Jamming is not just cool any more," *Nature*, vol. 396, pp. 21–22, nov 1998.

[2] A. A. Díaz and L. Trujillo, "Complex Fluids, Soft Matter and the Jamming Transition Problem," pp. 211–233, Springer, Cham, 2014.

[3] H. Princen, "Rheology of foams and highly concentrated emulsions: I. Elastic properties and yield stress of a cylindrical model system," *Journal of Colloid and Interface Science*, vol. 91, pp. 160–175, jan 1983.

[4] N. D. Denkov, S. Tcholakova, K. Golemanov, K. P. Ananthpadmanabhan, and A. Lips, "The role of surfactant type and bubble surface mobility in foam rheology," *Soft Matter*, vol. 5, p. 3389, sep 2009.

[5] J. Goyon, A. Colin, and L. Bocquet, "How does a soft glassy material flow: finite size effects, non local rheology, and flow cooperativity," *Soft Matter*, vol. 6, p. 2668, jun 2010.

[6] T. Mason, J. Bibette, and D. Weitz, "Yielding and Flow of Monodisperse Emulsions," *Journal of Colloid and Interface Science*, vol. 179, pp. 439–448, may 1996.

[7] D. Bonn, P. Coussot, H. T. Huynh, F. Bertrand, and G. Debrégeas, "Rheology of soft glassy materials," *Europhysics Letters (EPL)*, vol. 59, pp. 786–792, sep 2002.

[8] P. Coussot, "Yield stress fluid flows: A review of experimental data," *Journal of Non-Newtonian Fluid Mechanics*, vol. 211, pp. 31–49, sep 2014.

[9] Q. D. Nguyen and D. V. Boger, "Thixotropic behaviour of concentrated bauxite residue suspensions," *Rheologica Acta*, vol. 24, pp. 427–437, jul 1985.

[10] J. Goyon, A. Colin, G. Ovarlez, A. Ajdari, and L. Bocquet, "Spatial cooperativity in soft glassy flows," *Nature*, vol. 454, pp. 84–87, jul 2008.

[11] V. Mansard, L. Bocquet, and A. Colin, "Boundary conditions for soft glassy flows: slippage and surface fluidization," *Soft Matter*, vol. 10, pp. 6984–6989, apr 2014.

[12] L. Derzsi, D. Filippi, G. Mistura, M. Pierno, M. Lulli, M. Sbragaglia, M. Bernaschi, and P. Garstecki, "Fluidization and wall slip of soft glassy materials by controlled surface roughness," *Physical Review E*, vol. 95, no. 5, pp. 1–6, 2017.

[13] L. Derzsi, D. Filippi, M. Lulli, G. Mistura, M. Bernaschi, P. Garstecki, M. Sbragaglia, and M. Pierno, "Wall fluidization in two acts: From stiff to soft roughness," *Soft Matter*, vol. 14, no. 7, pp. 1088–1093, 2018.

[14] V. Mansard and A. Colin, "Local and non local rheology of concentrated particles," *Soft Matter*, vol. 8, no. 15, pp. 4025–4043, 2012.

[15] A. Björn, P. Segura, L. Monja, A. Karlsson, J. Ejlertsson, and B. H. Svensson, "3 Rheological Characterization," tech. rep.

[16] R. P. Chhabra, "Non-Newtonian Fluids : An Introduction," pp. 1–33.

[17] R. G. Larson, *The structure and rheology of complex fluids*. Oxford University Press, 1999.

[18] D. Filippi, *Local fluidization of concentrated emulsion in microfluidic channels textured at the droplet scale*. PhD thesis, Università degli studi di Padova, 2018.

[19] S. Vongvuthipornchai and R. Raghavan, "Well Test Analysis of Data Dominated by Storage and Skin: Non-Newtonian Power-Law Fluids," *SPE Formation Evaluation*, vol. 2, pp. 618–628, dec 1987.

[20] M. M. Cross, "Rheology of non-Newtonian fluids: A new flow equation for pseudoplastic systems," *Journal of Colloid Science*, vol. 20, pp. 417–437, jun 1965.

[21] H. A. Barnes, "The yield stressa review or $\pi\alpha\nu\tau\alpha$ $\rho\epsilon\iota$'everything flows?," *Journal of Non-Newtonian Fluid Mechanics*, vol. 81, pp. 133–178, feb 1999.

[22] J. F. Steffe, *Rheological methods in food process engineering*. Freeman Press, 1996.

[23] E. A. Toorman, "Modelling the thixotropic behaviour of dense cohesive sediment suspensions," *Rheologica Acta*, vol. 36, no. 1, pp. 56–65, 1997.

[24] I. Steg and D. Katz, "Rheopexy in some polar fluids and in their concentrated solutions in slightly polar solvents," *Journal of Applied Polymer Science*, vol. 9, pp. 3177–3193, sep 1965.

[25] K. N. Nordstrom, E. Verneuil, P. E. Arratia, A. Basu, Z. Zhang, A. G. Yodh, J. P. Gollub, and D. J. Durian, "Microfluidic Rheology of Soft Colloids above and below Jamming," *Physical Review Letters*, vol. 105, p. 175701, oct 2010.

[26] C. S. O'Hern, L. E. Silbert, A. J. Liu, and S. R. Nagel, "Jamming at zero temperature and zero applied stress: The epitome of disorder," *Physical Review E*, vol. 68, p. 011306, jul 2003.

[27] T. G. Mason, J. Bibette, and D. A. Weitz, "Elasticity of Compressed Emulsions," *Physical Review Letters*, vol. 75, pp. 2051–2054, sep 1995.

[28] M. J. Rosen and J. T. Kunjappu, *Surfactants and interfacial phenomena*. Wiley, 2012.

[29] F. Leal-Calderon, V. Schmitt, and J. Bibette, *Emulsion science : basic principles*. Springer, 2007.

[30] P. K. Kundu, I. M. Cohen, D. R. Dowling, and G. Tryggvason, *Fluid mechanics*.

[31] O. Reynolds, "An Experimental Investigation of the Circumstances Which Determine Whether the Motion of Water Shall Be Direct or Sinuous, and of the Law of Resistance in Parallel Channels," *Philosophical Transactions of the Royal Society of London*, vol. 174, no. 0, pp. 935–982, 1883.

[32] F. M. White, *Fluid mechanics*. McGraw-Hill, 2008.

[33] E. Lauga, M. Brenner, and H. Stone, "Microfluidics: The No-Slip Boundary Condition," in *Springer Handbook of Experimental Fluid Mechanics*, pp. 1219–1240, Berlin, Heidelberg: Springer Berlin Heidelberg, 2007.

[34] C. Neto, V. Craig, and D. Williams, "Evidence of shear-dependent boundary slip in newtonian liquids," *The European Physical Journal E*, vol. 12, pp. 71–74, nov 2003.

[35] C. Institute of Physics (Great Britain), D. R. Physical Society (Great Britain), E. Institute of Physics and the Physical Society., H.-J. Institute of Physics Publishing., and V. S. J. Craig, *Reports on progress in physics.*, vol. 68. The Institute of Physics.

[36] M. Sahraoui and M. Kaviany, "Slip and no-slip velocity boundary conditions at interface of porous, plain media," *International Journal of Heat and Mass Transfer*, vol. 35, pp. 927–943, apr 1992.

[37] S. Yordanov, A. Best, H.-J. Butt, and K. Koynov, "Direct studies of liquid flows near solid surfaces by total internal reflection fluorescence cross-correlation spectroscopy," tech. rep., 2009.

[38] R. Pit, H. Hervet, and L. Léger, "Direct Experimental Evidence of Slip in Hexadecane: Solid Interfaces," *Physical Review Letters*, vol. 85, pp. 980–983, jul 2000.

[39] D. C. Tretheway and C. D. Meinhart, "A generating mechanism for apparent fluid slip in hydrophobic microchannels," *Physics of Fluids*, vol. 16, pp. 1509–1515, may 2004.

[40] L. Bécu, P. Grondin, A. Colin, and S. Manneville, "How does a concentrated emulsion flow?: Yielding, local rheology, and wall slip," *Colloids and Surfaces A: Physicochemical and Engineering Aspects*, vol. 263, pp. 146–152, aug 2005.

[41] M. Sánchez, C. Valencia, J. Franco, and C. Gallegos, "Wall Slip Phenomena in Oil-in-Water Emulsions: Effect of Some Structural Parameters," *Journal of Colloid and Interface Science*, vol. 241, pp. 226–232, sep 2001.

[42] H. S. Tang and D. M. Kalyon, "Unsteady circular tube flow of compressible polymeric liquids subject to pressure-dependent wall slip," *Journal of Rheology*, vol. 52, pp. 507–525, mar 2008.

[43] B. K. Aral and D. M. Kalyon, "Effects of temperature and surface roughness on timedependent development of wall slip in steady torsional flow of concentrated suspensions," *Journal of Rheology*, vol. 38, pp. 957–972, jul 1994.

[44] R. J. Daniello, N. E. Waterhouse, and J. P. Rothstein, "Drag reduction in turbulent flows over superhydrophobic surfaces," *Physics of Fluids*, vol. 21, p. 085103, aug 2009.

[45] S. Varagnolo, D. Ferraro, P. Fantinel, M. Pierno, G. Mistura, G. Amati, L. Biferale, and M. Sbragaglia, "Stick-Slip Sliding of Water Drops on Chemically Heterogeneous Surfaces," *Physical Review Letters*, vol. 111, p. 066101, aug 2013.

[46] G. Ovarlez, Q. Barral, and P. Coussot, "Three-dimensional jamming and flows of soft glassy materials," *Nature Materials*, vol. 9, pp. 115–119, feb 2010.

[47] G. Picard, A. Ajdari, F. Lequeux, and L. Bocquet, "Elastic consequences of a single plastic event: A step towards the microscopic modeling of the flow of yield stress fluids," *The European Physical Journal E*, vol. 15, pp. 371–381, dec 2004.

[48] M. Bouzid, M. Trulsson, A. Izzet, A. Favier de Coulomb, P. Claudin, E. Clément, and B. Andreotti, "Non-local rheology of dense granular flows," *EPJ Web of Conferences*, vol. 140, p. 11013, jun 2017.

[49] J. Paredes, N. Shahidzadeh, and D. Bonn, "Wall slip and fluidity in emulsion flow," *Physical Review E*, vol. 92, p. 042313, oct 2015.

[50] M. Sbragaglia, R. Benzi, M. Bernaschi, and S. Succi, "The emergence of supramolecular forces from lattice kinetic models of non-ideal fluids: applications to the rheology of soft glassy materials," *Soft Matter*, vol. 8, p. 10773, oct 2012.

[51] L. Bocquet, A. Colin, and A. Ajdari, "Kinetic Theory of Plastic Flow in Soft Glassy Materials," *Physical Review Letters*, vol. 103, p. 036001, jul 2009.

[52] W. D. Bancroft, "The Theory of Emulsification, V," *The Journal of Physical Chemistry*, vol. 17, pp. 501–519, jan 1912.

[53] H. Karbstein and H. Schubert, "Developments in the continuous mechanical production of oil-in-water macro-emulsions," *Chemical Engineering and Processing: Process Intensification*, vol. 34, pp. 205–211, jun 1995.

[54] J. Sjoblom, *Emulsions and emulsion stability*. Taylor & Francis, 2006.

[55] J.-Y. Tinevez, N. Perry, J. Schindelin, G. M. Hoopes, G. D. Reynolds, E. Laplantine, S. Y. Bednarek, S. L. Shorte, and K. W. Eliceiri, "TrackMate: An open and extensible platform for single-particle tracking," *Methods*, vol. 115, pp. 80–90, feb 2017.

[56] J. Schindelin, I. Arganda-Carreras, E. Frise, V. Kaynig, M. Longair, T. Pietzsch, S. Preibisch, C. Rueden, S. Saalfeld, B. Schmid, J.-Y. Tinevez, D. J. White, V. Hartenstein, K. Eliceiri, P. Tomancak, and A. Cardona, "Fiji: an open-source platform for biological-image analysis," *Nature Methods*, vol. 9, p. 676, jun 2012.